UM-016968-F

(12)

FINAL REPORT

Detonation Characteristics of Some Dusts and Liquid-Dust Suspensions

by

C. W. Kauffman
J. A. Nicholls
M. Sichel
P. Lee
D. Lee

Gas Dynamics Laboratories
Department of Aerospace Engineering
The University of Michigan
Ann Arbor, Michigan 48109-2140

Prepared for

Directorate of Aerospace Sciences
Air Force Office of Scientific Research (AFSC)
Bolling Air Force Base, D. C. 20332

July 1983

UNCLASSIFIED

SECURITY CLASSIFICATION OF THIS PAGE

AD-A148735

REPORT DOCUMENTATION PAGE

1a. REPORT SECURITY CLASSIFICATION UNCLASSIFIED	1b. RESTRICTIVE MARKINGS
2a. SECURITY CLASSIFICATION AUTHORITY	3. DISTRIBUTION/AVAILABILITY OF REPORT Approved for public release; Distribution is Unlimited
2b. DECLASSIFICATION/DOWNGRADING SCHEDULE	
4. PERFORMING ORGANIZATION REPORT NUMBER(S) UM-016968-F	5. MONITORING ORGANIZATION REPORT NUMBER(S) AFOSR-TR- 84-1130
6a. NAME OF PERFORMING ORGANIZATION The University of Michigan 6b. OFFICE SYMBOL (If applicable)	7a. NAME OF MONITORING ORGANIZATION AFOSR/NA
6c. ADDRESS (City, State and ZIP Code) Department of Aerospace Engineering Ann Arbor, MI 48109-2140	7b. ADDRESS (City, State and ZIP Code) Bolling AFB, D.C. 20332
8a. NAME OF FUNDING/SPONSORING ORGANIZATION AIR FORCE OFFICE OF SCIENTIFIC RESEARCH 8b. OFFICE SYMBOL (If applicable) NA	9. PROCUREMENT INSTRUMENT IDENTIFICATION NUMBER AFOSR-79-0093
8c. ADDRESS (City, State and ZIP Code) BOLLING AFB DC 20332-6600	10. SOURCE OF FUNDING NOS. PROGRAM ELEMENT NO.: 61102F PROJECT NO.: 2308 TASK NO.: A2 WORK UNIT NO.:
11. TITLE (Include Security Classification) DETONATION CHARACTERISTICS OF SOME DUSTS AND LIQUID-DUST SUSPENSIONS	
12. PERSONAL AUTHOR(S) C W KAUFFMAN; J A NICHOLLS; M SICHEL; P LEE; D LEE	
13a. TYPE OF REPORT FINAL 13b. TIME COVERED FROM 01MAR79 TO 01MAY83	14. DATE OF REPORT (Yr., Mo., Day) JULY 1983 15. PAGE COUNT
16. SUPPLEMENTARY NOTATION	
17. COSATI CODES FIELD / GROUP / SUB. GR.	18. SUBJECT TERMS (Continue on reverse if necessary and identify by block number) HETEROGENEOUS DETONATION DUST EXPLOSIONS FUEL AIR EXPLOSIONS
19. ABSTRACT (Continue on reverse if necessary and identify by block number) (SEE REVERSE)	
20. DISTRIBUTION/AVAILABILITY OF ABSTRACT UNCLASSIFIED/UNLIMITED ☒ SAME AS RPT. ☐ DTIC USERS ☐	21. ABSTRACT SECURITY CLASSIFICATION UNCLASSIFIED
22a. NAME OF RESPONSIBLE INDIVIDUAL JULIAN M TISHKOFF	22b. TELEPHONE NUMBER (Include Area Code) (202) 767-4935 22c. OFFICE SYMBOL AFOSR/NA

DD FORM 1473, 83 APR EDITION OF 1 JAN 73 IS OBSOLETE.

UNCLASSIFIED

SECURITY CLASSIFICATION OF THIS PAGE

84 12 17 014

The detonation characteristics of high explosive dusts dispersed in air were studied in a special "shock tube type" facility wherein the dust was transported through the tube by a gas flow. Detonation of high pressure gases in the driver served to transmit a strong blast wave into the dust mixture. The resultant wave was monitored by pressure switches, pressure transducers, a photodiode, and streak photography. RDX dust in air could not be detonated. However, detonation was realized with 150-micrometre diameter particles in oxygen-enriched air. The small RDX particles (10 micrometre) could not be detonated, even with the oxygen enrichment. The conclusion drawn was that the inertia of the large particles led to a large relative velocity between the particles and gas behind the shock wave with the attendant high stagnation temperature and rapid heating to ignition. Other experiments were conducted wherein excess oxygen was supplied by the addition of ammonium perchlorate dust, AP, to the RDX. The AP did increase the sensitivity and some detonation results are presented. Experiments were conducted on the shock wave ignition characteristics of liquid fuel drops with entrained small dust particles. The liquid fuel used was decane and the dusts included RDX, AP and inert aluminum oxide. In general, these dusts served to decrease the ignition time delay and hence to increase the detonability. A theoretical model was developed for the ignition time delay of dust particles behind a shock wave and gave good agreement with experiment results. An approximate model for the combustion rate of dust, derived in part from the experiments, predicted the propagation rate and structure of a steady state dust detonation. Numerical calculations were made on the unsteady propagation of a dust detonation when initiated by a blast wave.

UM-016968-F

FINAL REPORT

Detonation Characteristics of Some Dusts and Liquid-Dust Suspensions

by

C. W. Kauffman
J. A. Nicholls
M. Sichel
P. Lee
D. Lee

Gas Dynamics Laboratories
Department of Aerospace Engineering
The University of Michigan
Ann Arbor, Michigan 48109-2140

Prepared for

Directorate of Aerospace Sciences
Air Force Office of Scientific Research (AFSC)
Bolling Air Force Base, D. C. 20332

July 1985

PREFACE

This research was conducted at the Gas Dynamics Laboratory, Department of Aerospace Engineering, The University of Michigan, under AFOSR Grant 79-0093 over the time period 1 March 1979 through 30 April 1983. Professors J. A. Nicholls and M. Sichel and Dr. C. W. Kauffman served as senior investigators. Dr. B. T. Wolfson, Directorate of Aerospace Sciences, Air Force Office of Scientific Research served as Project Manager for the Air Force for all but the last few months of the program. Dr. Julian Tishkoff served in that capacity for the final few months.

In the earlier stages of the program, significant contributions were made by D. R. Glass, Research Scientist; J. Draxler and D. Purmort, graduate students; and K. Wood, an undergraduate student.

TABLE OF CONTENTS

LIST OF FIGURES

LIST OF TABLES

I. INTRODUCTION

Condensed explosives are commonly used for commercial applications as well as by the Department of Defense. In the condensed form, solid or liquid, these explosives are made to detonate through use of a suitable initiator. For many of these explosives, the detonation velocities and pressures have been calculated and measurements have been made which are in reasonable agreement with the theory. An interesting ramification of this for solid explosives is that wherein the explosive is in the form of a dust and is dispersed in a gaseous oxidizer, such as air. These dusts are monopropellants (containing C, H and O) and, hence, the question arises as to whether the individual particles will detonate when subjected to a strong shock wave with subsequent reaction of the combustion products with the atmosphere. The other possibility is that the particles do not detonate individually but rather, just burn with the surrounding gas. However, it is possible that the overall process could still propagate as a supersonic combustion wave; that is, a "dust detonation."

The overall aim of this research investigation was, then, to determine the detonation characteristics of high explosive dusts dispersed in a gaseous oxidizing medium. The thrust of the program was to determine whether the dust cloud could detonate, the pressures and velocities developed, the reaction mechanism, the limits of detonation, the influence of particle size and concentration, initiation energy required, etc. In order to generate this knowledge with a high degree of confidence, it was deemed essential to conduct a well controlled experimental investigation along with a closely related analytical treatment. Towards this end, a special research facility was developed which allowed one dimensional waves to propagate through a dust cloud. Plastic coated RDX (Trinitro-Triazacyclohexane) dust was tested in air, oxygen enriched air, and in nitrogen. Some experiments utilized AP (ammonium perchlorate) dust or the inert dust, Al_2O_3, mixed in with the RDX. Other experiments investigated the shock wave ignition

of decane droplets with entrained RDX particles. On the analytical side, attention was given to the steady detonation and structure of such dust detonations, blast wave initiation, and the ignition of dust particles behind the lead shock.

The experimental aspects of the program will now be described in some detail, followed by a discussion of the analytical studies.

II. EXPERIMENTAL STUDIES

The experimental determination of the detonation characteristics of heterogeneous detonation is, of course, much more difficult than with gaseous mixtures. The observation distance of the propagating wave must be relatively long and a uniform dispersion of the dust in the gas is required in order to get steady state conditions. Recognizing that dust detonations are, in general, harder to initiate, it was decided to use blast wave initiation. Accordingly, a special horizontal shock tube was designed and built wherein the dust was entrained and transported along the tube by the oxidizing gas. At the appropriate time, a strong, blast wave was transmitted into this flowing mixture. Measurements were then made to determine the detonation characteristics. In other tests, this facility was used to study the shock wave ignition of a liquid fuel droplet with entrained combustible dust. The main parts of the facility are described in the following sections.

A. EXPERIMENTAL FACILITY

1. Shock Tube

Figure 1 is a schematic diagram of the horizontal shock tube which indicates the major dimensions and various components. The driver section, which is separated from the transition section by a diaphragm, consists of a 5-ft. length of 2-7/8 in. I. D. schedule 80 seamless stainless steel pipe. It can be charged with a high pressure hydrogen-oxygen-helium ($2H_2 + O_2 + He$) gas mixture which can be detonated and thus transmit a strong blast wave into the flowing dust gaseous mixture. For other experiments, the driver section can be charged with high pressure helium (up to 3000 psi) for conventional shock tube operation.

The 5-ft. long driver is more than is necessary in terms of testing time and initiation energy for both modes of operation. Therefore, three-fourths of the driver length is plugged with volume spacers to reduce the available

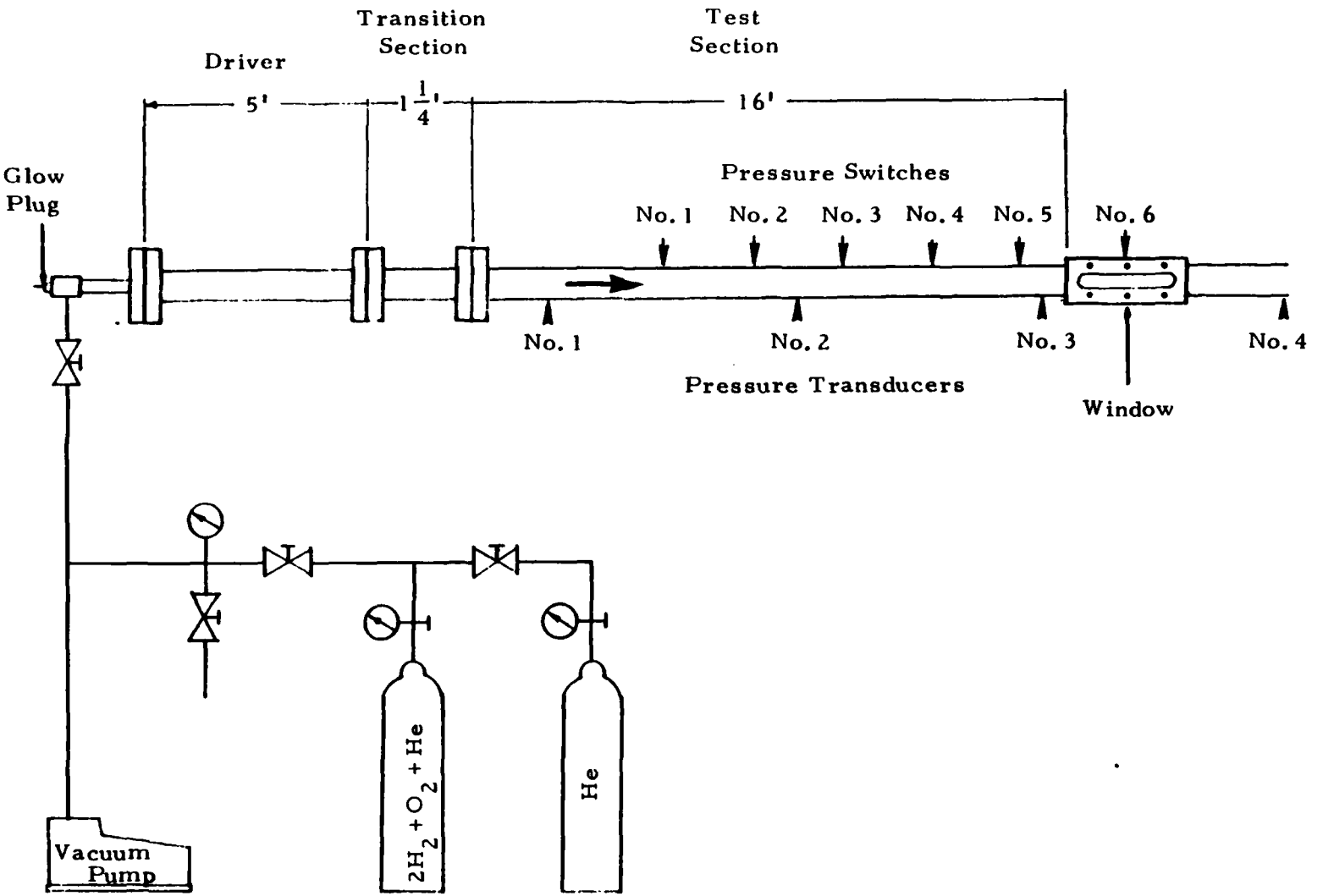

Figure 1. Schematic Diagram of Shock Tube.

driver and driver gas to a quarter of the full volume, as shown in Fig. 2. The three spacers are made of cast aluminum, 1.25-ft. in length. During the discharge of the driver when filled with 3000 psi helium, a differential force of 14,000 lb. acts on the spacers and could tend to fire the spacers into the shock tube. Therefore, a heavy scheduled steel pipe of 1.315 in. O.D. and 0.56 in. I.D. is used to hold the spacers securely. The pipe is threaded into the end flange of the driver at one end and with a jam nut at the other end in order to restrain the spacers from being dislodged. The driver is supported on a roller so that it can be moved back from the transition section to facilitate the installation and removal of the diaphragm between the flanges.

The transition section adapts the circular driver to the rectangular driven section; there is a 47% reduction in area. A dust feeder is mounted on top of it to introduce dust into the shock tube, as shown in Fig. 3. Two side jets with 0.0064 in. nozzles are also mounted on each side of the transition section to inject gaseous oxidizer and carry the entering dust into the driven section.

The driven section (test section) of the shock tube is a 20-ft. long rectangular seamless stainless steel tube with internal dimensions of 1.5 in. x 2.5 in. and a wall thickness of 3/8 in. One end of this section is flanged to the transition section and the other end open to the atmosphere. Holes are drilled and threaded along the tube to adapt various sensing devices. The window is located 16-ft. from the transition section. Schlieren quality windows, 6 in. long, 1 in. wide and 15/16 in. thick, are held in two rectangular flanges which fit into the slots cut in both sides of the shock tube.

2. Dust Feeder

The dust is introduced into the tube with the dust feeder, which consists of a brass feeding block, a feeding cartridge with plunger, a driver triggering switch, and a constant speed pulling motor. The brass feeding block, shown in Fig. 4, has the dust feeding cartridge on one side. At the

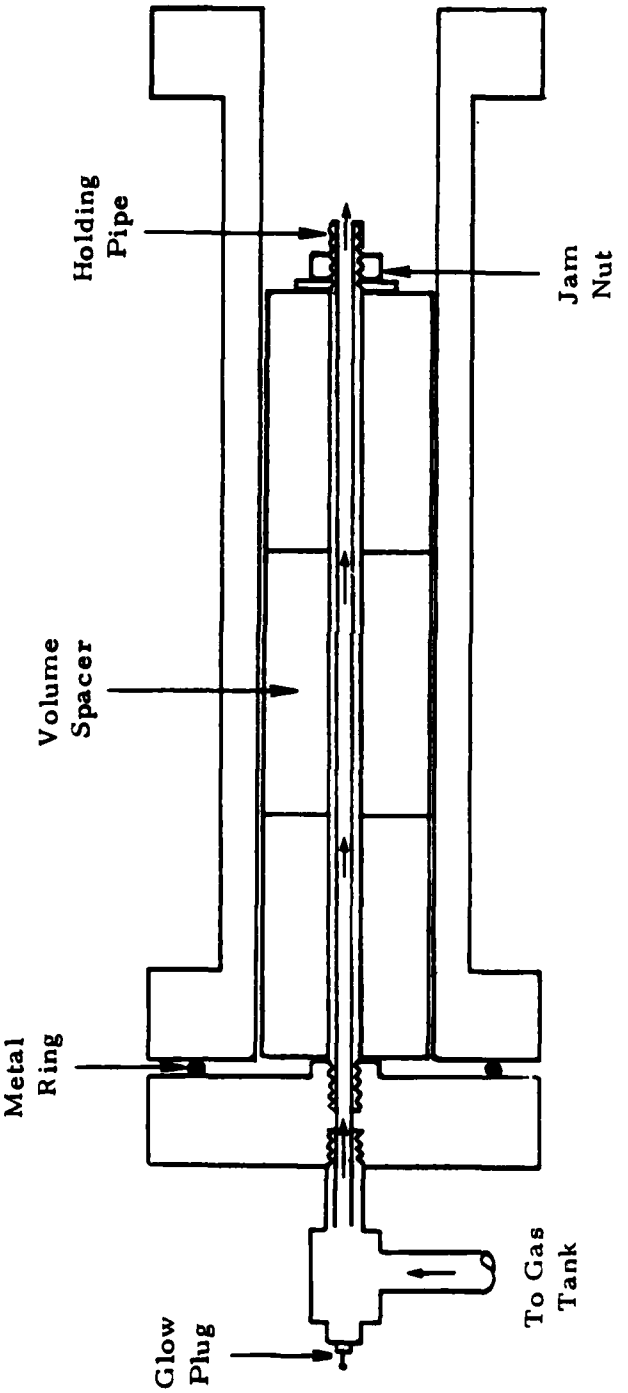

Figure 2. Driver Cross Section.

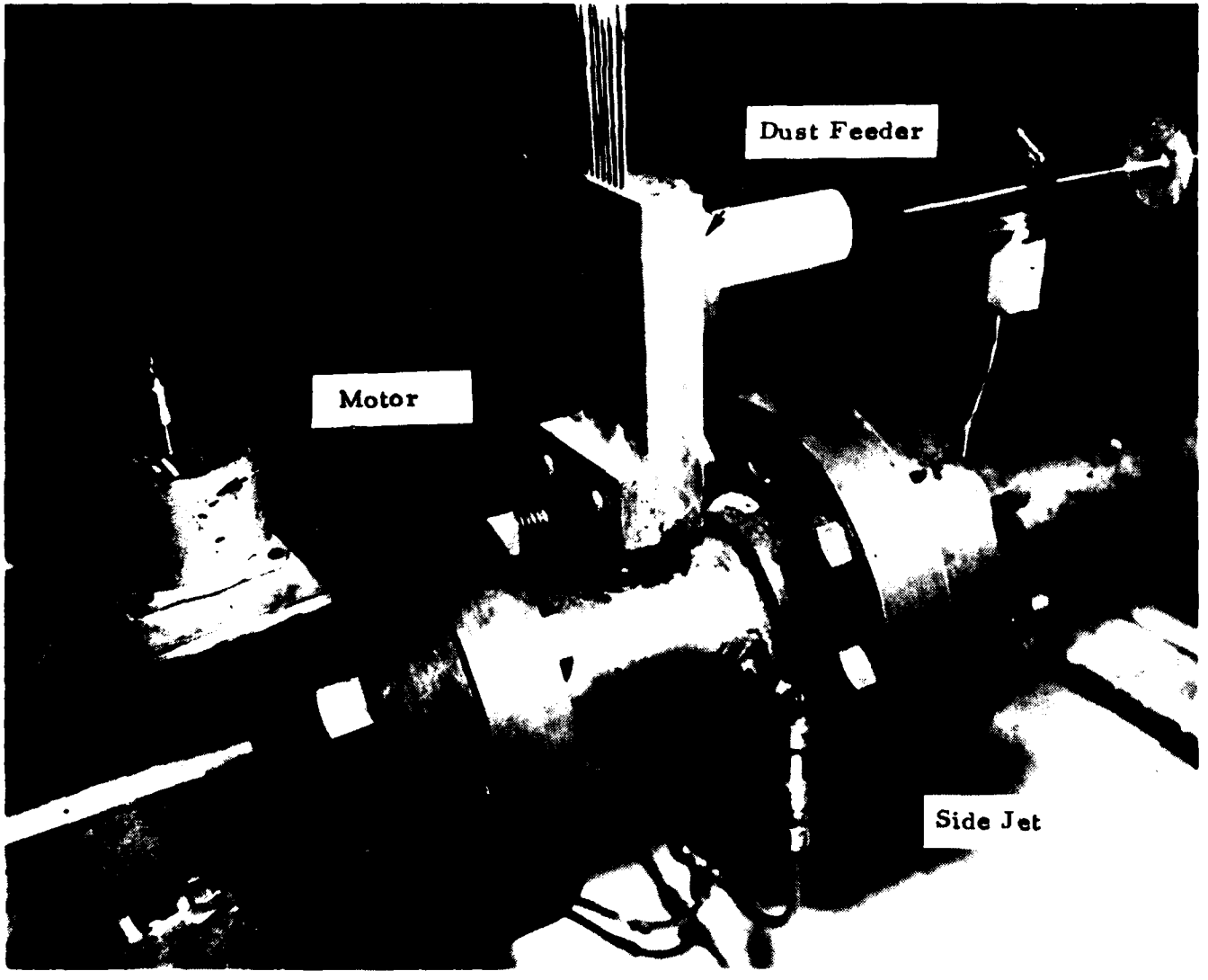

Figure 3. Transition Section and Dust Feeder.

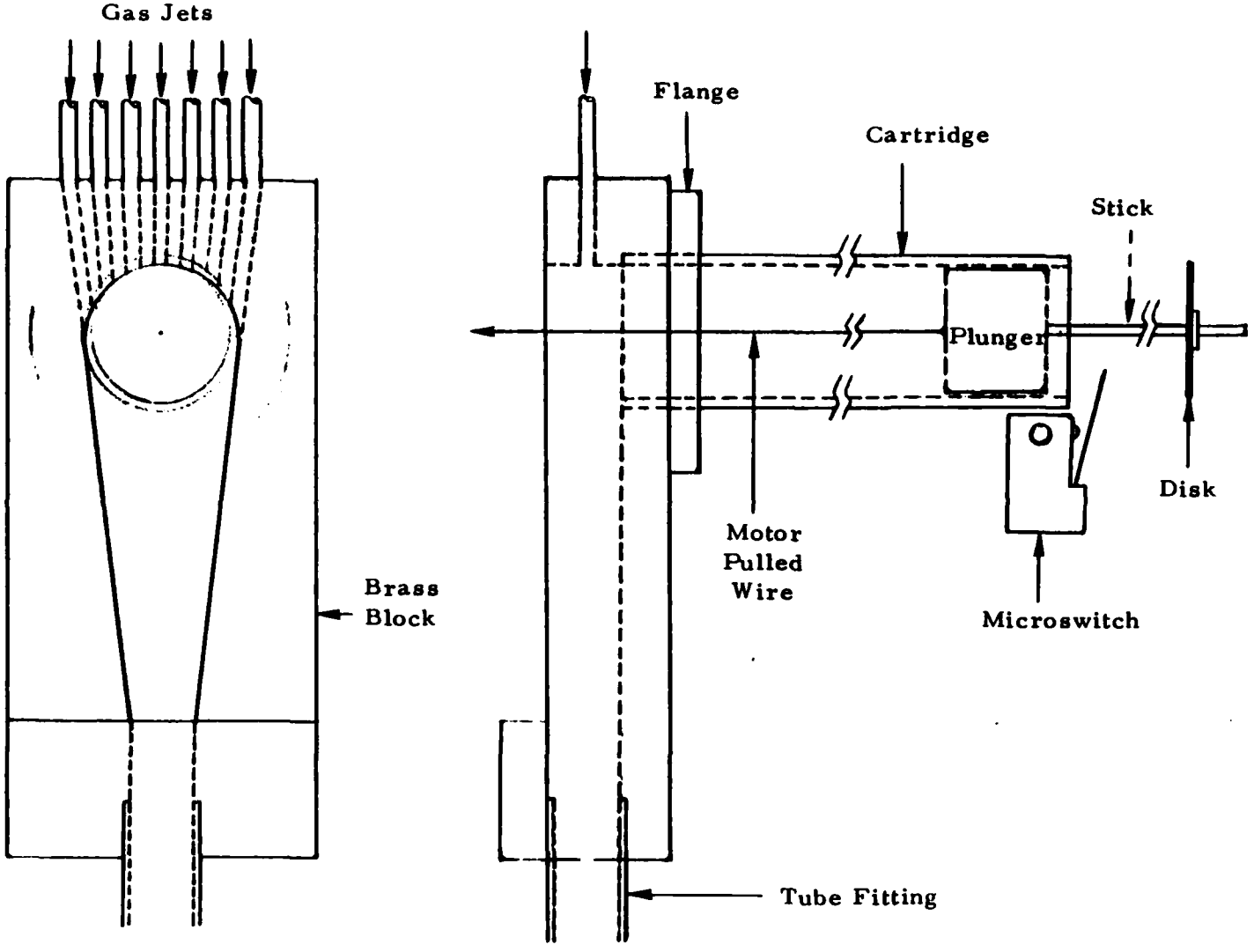

Figure 4. Dust Feeder.

top seven gas jets are introduced which carry the dust into the transition section. A pipe fitting at the bottom of the feeding block attaches the feeder to the transition section and allows the dust to be introduced. During operation, the motor pulls the plunger in the feeding cartridge by use of a wire, thereby forcing the dust into the brass block. The dust is forced into the transition section and de-agglomerated by the seven air jets. When the plunger reaches the end of the feeding cartridge and all of the dust has been fed into the transition section, the disc, mounted on the plunger, actuates the glow plug trigger switch to detonate the driver.

The open side of the brass feeding block is tape-sealed with a mylar diaphragm. Upon firing of the driver, the pressure is increased in the dust feeder which is then released by rupture of the mylar diaphragm. Therefore, the damage done to the dust feeder is minimized. The dust feeding cartridge, which is made with an acrylic tube and able to last for several runs before it is shattered and burned, is replaced frequently. The constant speed pulling motor has a multi-staged pulley on its shaft so that it can pull the plunger at various dust feeding rates which, coupled with various gaseous oxidizer flow rates, gives the desired dust concentration in the shock tube. The seven gas jets in the top of the brass feeding block have a nozzle of 2.89×10^{-6} ft.^{2} each and contribute a small portion of the gaseous oxidizer flow. The major part of the gas flow, which transports the dust down the tube, comes from the two side jets mounted on each side of the transition section.

3. Instrumentation

The important events, such as wave speed, pressure, light emission, droplet shattering, and ignition in the various experiments are detected by the use of instrumentation which includes pressure switches, pressure transducers, a photodiode, and streak photography.

The pressure switch, which is a mechanical on/off electric switch activated by the pressure jump across the shock wave, is used to detect

the shock wave arrival time and hence, the speed. The pressure switch consists of a thin stainless steel diaphragm and a brass rod connected to electronic circuitry. Upon exposure to the sudden high pressure, the diaphragm deflects and makes an electrical contact with the brass rod with a response time of 1-2 microseconds. Several microsecond time counters are employed in conjunction with the pressure switches to count the shock wave travel times.

The shock wave pressures are sensed by a number of Kistler 603A quartz pressure transducers, which have a response time of one microsecond and pressure range of 3000 psi. The output charge of the pressure transducers is linearly proportional to the pressure and is amplified by a charge amplifier. A Tektronix 555 oscilloscope records the amplified outputs in terms of time history traces. The same oscilloscope also records the output of a Texas Instruments TL400 Photocell. The photocell has a response time of one microsecond and is located at the same position as the No. 3 pressure transducer shown in Fig. 1. The use of the photocell allows the measurement of the delay time between the shock and flame front.

Streak Schlieren photographs of dust detonations and droplet-shock-wave interactions are taken with a high speed drum camera and an optical setup as shown in Fig. 5. The light spark from a Xenon lamp located at the focus point of an 8-in. diameter concave mirror is reflected and collimated through a slit mounted on the camera side of the window. The transmitted light is then reflected from the second concave mirror and focuses on a vertical knife edge, whereas the image of the object inside the window focuses on the film in the drum camera through a lens. The Xenon light is triggered by the pressure switch located upstream of the window section. A time delay device is used in conjunction with the pressure switch and the light source power supply. When the pressure switch is swept by the shock wave, a signal is sent to the delay unit which delays the triggering of the light until the shock reaches the window section.

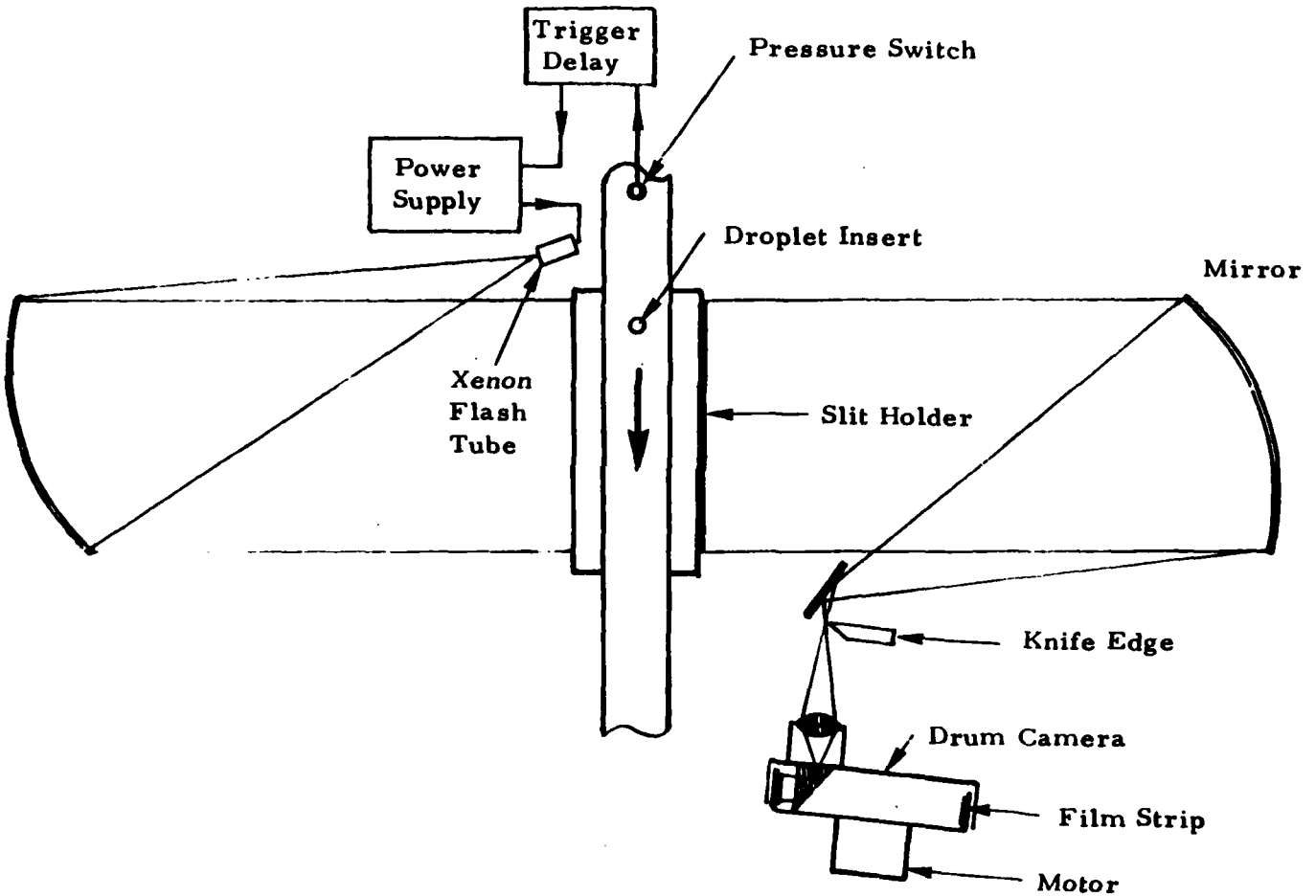

Figure 5. Optical Setup

4. Experimental Procedure

Since there are two kinds of experiments, RDX dust detonation and RDX decane droplet ignition, conducted in the same facility, the experimental procedures differed.

In the dust detonation runs, the explosive dust used is plastic coated RDX-E and RDX-A, where the former has an average particle size of 10 micrometers and the latter of 150 micrometers. The formula for RDX is $C_3H_6O_6N_6$. Electronic micrographs of the two sizes are shown in Fig. 6. The RDX-E dust is mixed with a small amount (2%) of amorphous fumed silica dust, known as Cab-O-Sil (C.O.S), to improve the dispersion characteristics of the dust along the tube.

The mylar diaphragm is inserted between the flanges that separate the driver and transition sections. The driver is evacuated first with a vacuum pump, then charged with $2H_2 + O_2$ + He gaseous mixture. The gaseous oxidizer is injected through the two side jets in the transition section and the seven dust carrier jets on the top of the brass dust feeding block. The volume flow rate of the gas must be high enough to keep the dust suspended and is regulated by the jet nozzle areas and the upstream pressure of the nozzles. The dust feeding cartridge is loaded with RDX dust and the motor's pulley diameter is selected for the desired dust feeding rate.

The dust concentration in the shock tube is then the ratio of dust feeding and total gas flow rates, wherein the volume occupied by the dust particles is neglected. The amount of dust loaded in the feeding cartridge has to be such that the dust feeding time is long enough to allow the dust cloud to be distributed to the full length of the driven section before the driver is fired. The drum camera, loaded with a strip of Kodak Tri-X pan film, is turned on and the light source power supply is energized to be triggered by the No. 5 pressure switch. The pressure switches are reset for every run and the pressure transducer charge amplifiers regrounded to eliminate the static charge buildup. The trace trigger level of the oscilloscope is set to be triggered by the No. 1 pressure

RDX-A 80X

RDX-E 80X

Figure 6. Electron Micrographs.

transducer. At this stage, the firing switch is turned on which starts the pulling motor to feed in the dust for several seconds. When the plunger reaches the end, the glow plug trigger switch is triggered by the disc mounted on the plunger and the driver is detonated.

In the single droplet ignition runs, the transition section is included as part of the driver and the dust feeder side jets are blocked. The available driver length is then nearly doubled so that the testing time at a window section is approximately 1 millisecond. Two sizes of droplets are tested, 2000 micrometers and 3000 micrometers. The droplet is suspended on the looped end of a thin cooper wire and is inserted into the shock tube through a hole on top of the window section. The droplet is suspended at the height of the slit for streak photography. The incident shock wave is produced by helium gas in the driver section. Steel shim stock, 0.008-0.02 in. thick and scored by a glass cutter, is used as the diaphragm material. A combination of the diaphragms in various thicknesses for a desired shock wave strength is put between the flanges that separate the transition and driven sections. Pure oxygen is used as the oxidizer and is injected into the shock tube from a hole in the front portion of the driven section. The driver is slowly charged with high pressure helium until the diaphragm is ruptured. A streak photograph is taken to provide the detailed information of shock wave-droplet interaction.

B. EXPERIMENTAL RESULTS

1. Preliminary Dust Detonation Experiments

Before making a systematic study of RDX dust detonations, a preliminary investigation of the combustion characteristics of RDX as compared to wheat and coal dusts was conducted. The ignition delay times of these dust clouds, an important aspect of detonability, were obtained in a horizontal shock tube in air and an Arrhenius plot was used to fit the

data and thus give an effective activation energy. The ignition delays shown in Fig. 7 where T_2 is the temperature behind the shock, reveal that RDX is somewhat more reactive than Pittsburg coal but much less reactive than wheat. The calculated activation energy of RDX dust is 62.7 KJ/mole.

Some dust detonation runs were then made with wheat and RDX in oxygen enriched air (O_2/air, 20/80). Figure 8 shows the comparison of these two dust runs with a pure blast wave, wherein the initiation energy conditions in the driver were the same in each case. The time-distance trajectories indicate that chemical reaction of the dust is helping to drive the wave. Obviously, the blast wave is decaying (slowing down) with distance, as it should. The same is true of the wheat/air case so it is not detonating. The RDX/air run seemingly attains a constant velocity and, hence, is close to detonation. However, pressure records indicate that it is probably not detonating.

In order to get guidance on the initiation energies to be used in the driver, calculations were made as to the critical radius, R*. This radius represents that distance where the energy released by combustion to that point is equal to the energy of the initiating source. If this value is too high, then a steady state detonation would never be observed within the tube length available. On the other hand, if it is too low detonation would not even be established. The expression for this critical radius is

$$R^* = (E/K_\nu \rho_o Q)^{1/\nu}$$

The factors ν and K_ν are geometric variables and are 1, 2, 3 and 1, 2, and 4 respectively for plane, cylindrical and spherical waves. In the present one-dimensional case, $\nu = K_\nu = 1$, E is the energy released by the initiator per unit cross sectional area of the shock tube, ρ_o is the density of the unburned fuel-oxidizer mixture, and Q is the heat released per unit mass of combustible mixture. In order to determine Q, a theoretical calculation of oxidizer/fuel mass ratio versus equivalence ratio, ϕ, based on the definition of ϕ in the NASA Equilibrium Chemistry computer program [1], was made. Q was then calculated. The results are shown in Fig. 9. The critical radius R* versus ϕ and driver pressure is listed in Table I.

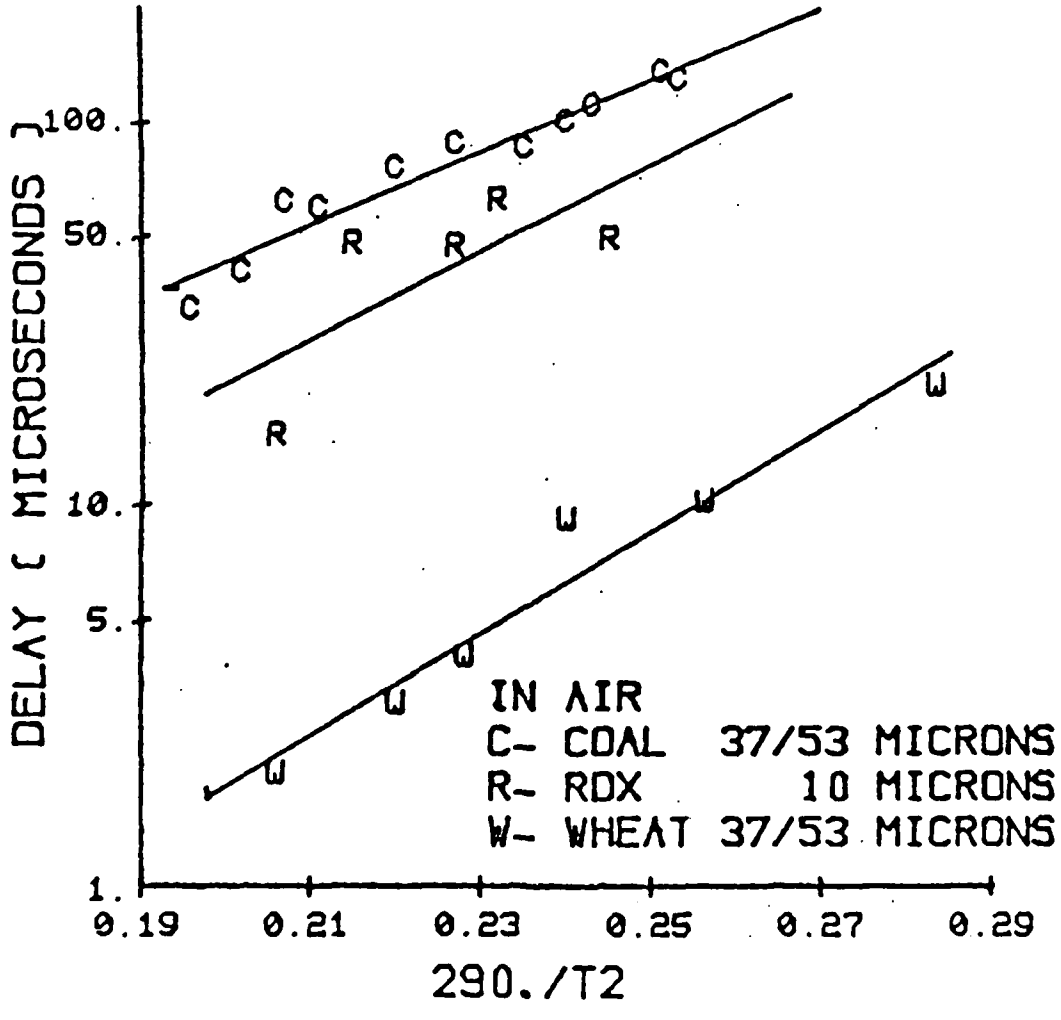

Figure 7. Ignition Time Delay of RDX, Coal and Wheat.

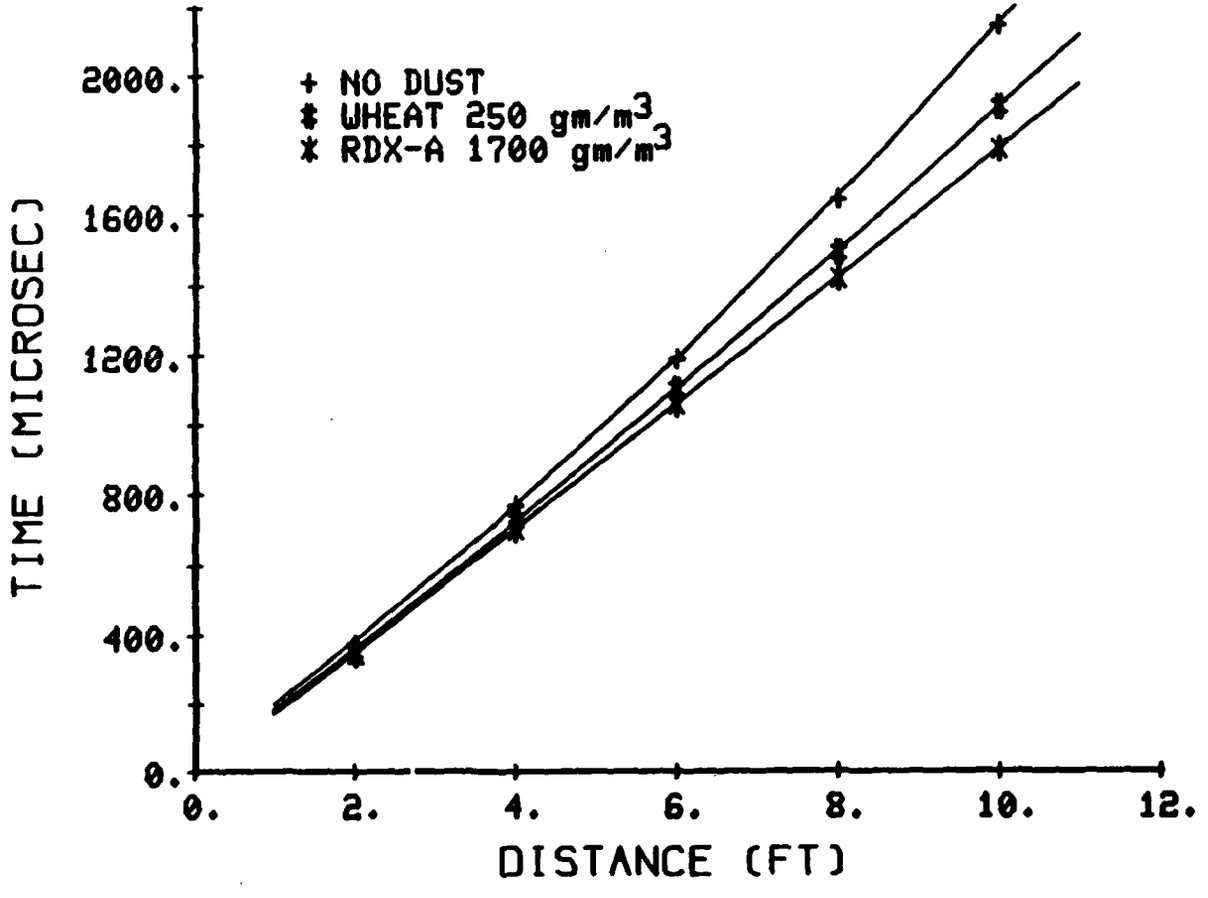

Figure 8. Detonation Runs of Some Dusts in Air/Oxygen (80/20) .

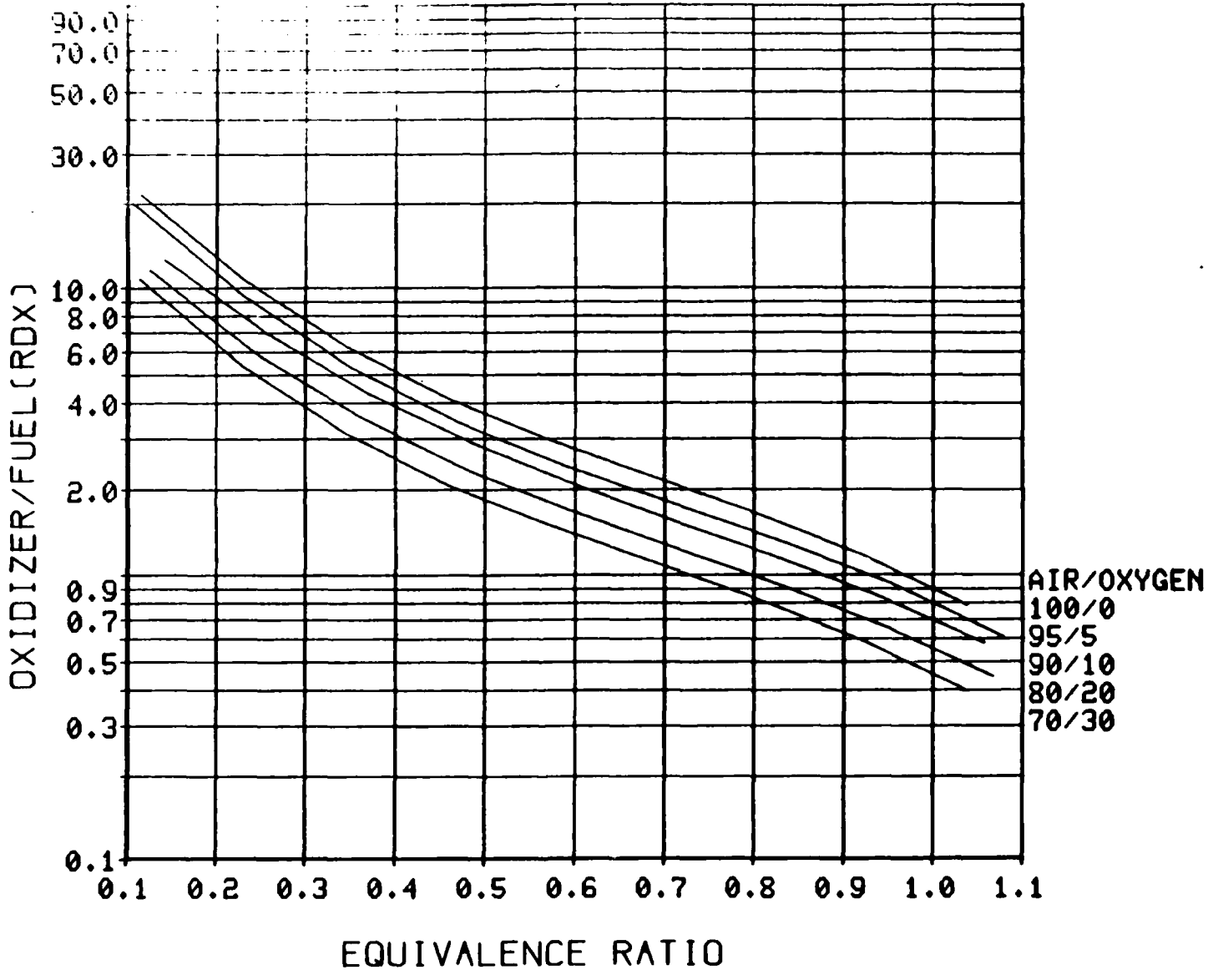

Figure 9. Oxidizer/ RDX Mass Ratios for Various Equivalence Ratios and Atmospheres.

Table I. Critical Radius for Various Operating Conditions.

Oxidizer = Air	Driver pressure (psig)	Critical Radius (m)
$\phi = .8$ $\rho_o = 2172.2$ $Q = 924.9$	60	2.2
	90	3.1
	105	3.5
	130	4.2
$\phi = .9$ $\rho_o = 2353.3$ $Q = 1029.5$	60	1.8
	90	2.5
	105	2.8
	130	3.5
$\phi = 1.0$ $\rho_o = 2715.3$ $Q = 1196.9$	60	1.3
	90	1.9
	105	2.2
	130	2.6

ϕ = Equivalence ratio

ρ_o = Density of RDX-Oxidizer Mixture (gm/m^3)

Q = = Heat of Combustion of RDX-Oxidizer mixture (Cal/ gm)

At a driver pressure of 105 psig, which had been used for most of the experiments, R* should be realized within half the length of the driven section. However, it does not follow that detonation will necessarily be established.

Along with the experimental runs, theoretical calculations, such as equivalence ratio, detonation velocity and pressure, were frequently acquired from the NASA Gordon-McBride computer program [1] for the purpose of precalculation and comparison.

The experimental results obtained are, for convenience, divided into the following categories:

Detonation of RDX in a Gaseous Oxidizer

Detonation of RDX/ AP in Air

Detonation of Aged RDX

Ignition of Liquid/ Dust Drops.

These results will now be presented.

2. Detonation of RDX in a Gaseous Oxidizer

RDX-A (large particles, 150 μm) were tested in various gases. Figure 10 shows Mach No. distance curves in cases where detonation was not achieved. The waves are decaying as they proceed along the shock tube. The only time detonation was experienced was in oxygen enriched air (88% air, 12% oxygen) and with a dust concentration of 1300 gm/m^3. The equivalence ratio, according to Fig. 9, was 0.86. Time-distance trajectories for stabilized wave patterns that had fairly constant wave speeds are shown in Fig. 11. The Mach number and pressure ratio near the end of the shock tube was approximately 5.1 and 32, respectively (Fig. 12). In comparison with the theoretical values, the experimental velocity and pressure results are 13% and 17% lower respectively, as shown in Fig. 13. The oscilloscope traces of a detonating and a non-detonating run are also compared in Fig. 14. In the detonating run the pressure rises are higher, and remain high while the ignition delay is shorter. Since RDX is a monopropellant, combustion does occur in N_2, but, as can be seen,

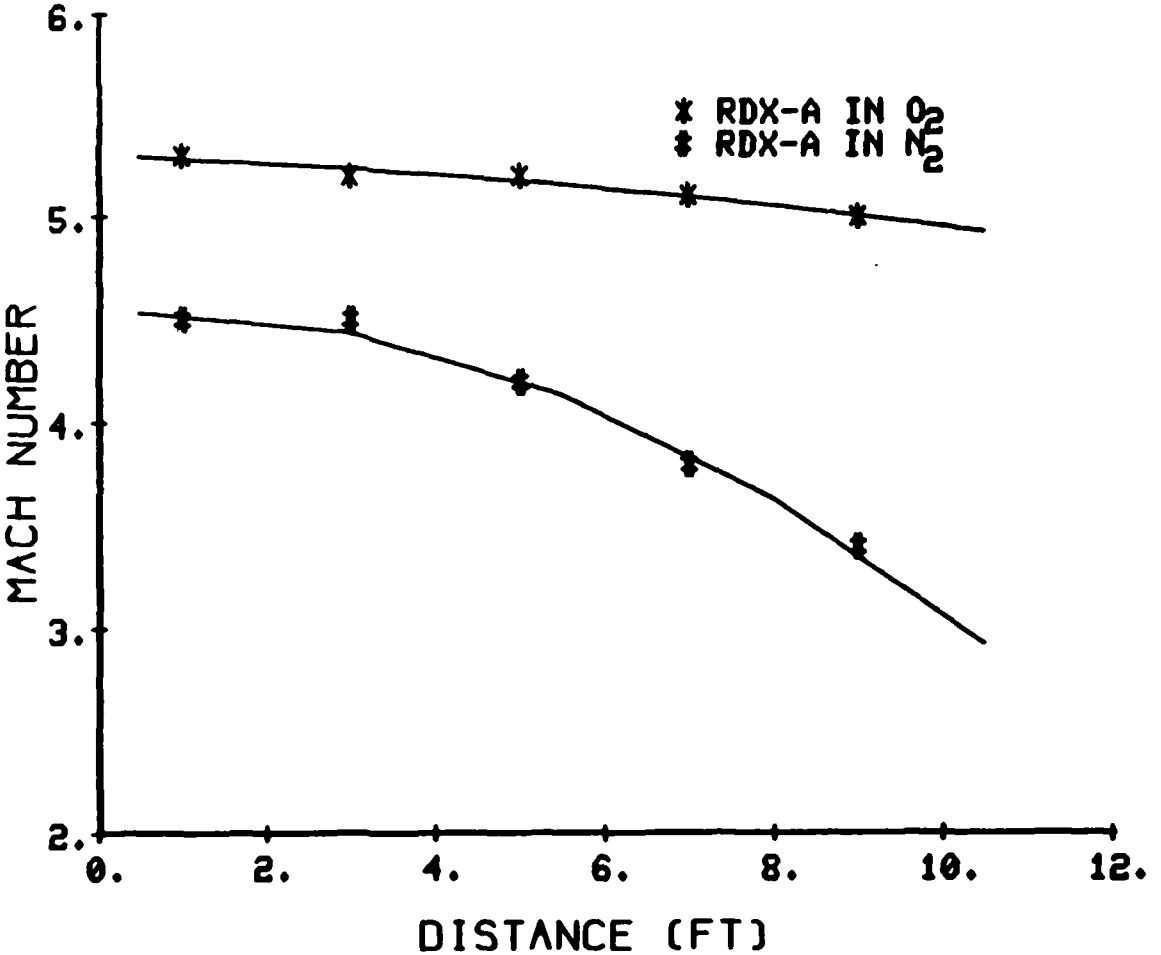

Figure 10. Detonation Runs of RDX-A, 1300 gm/m^3, Drive Pressure 119.3 psia .

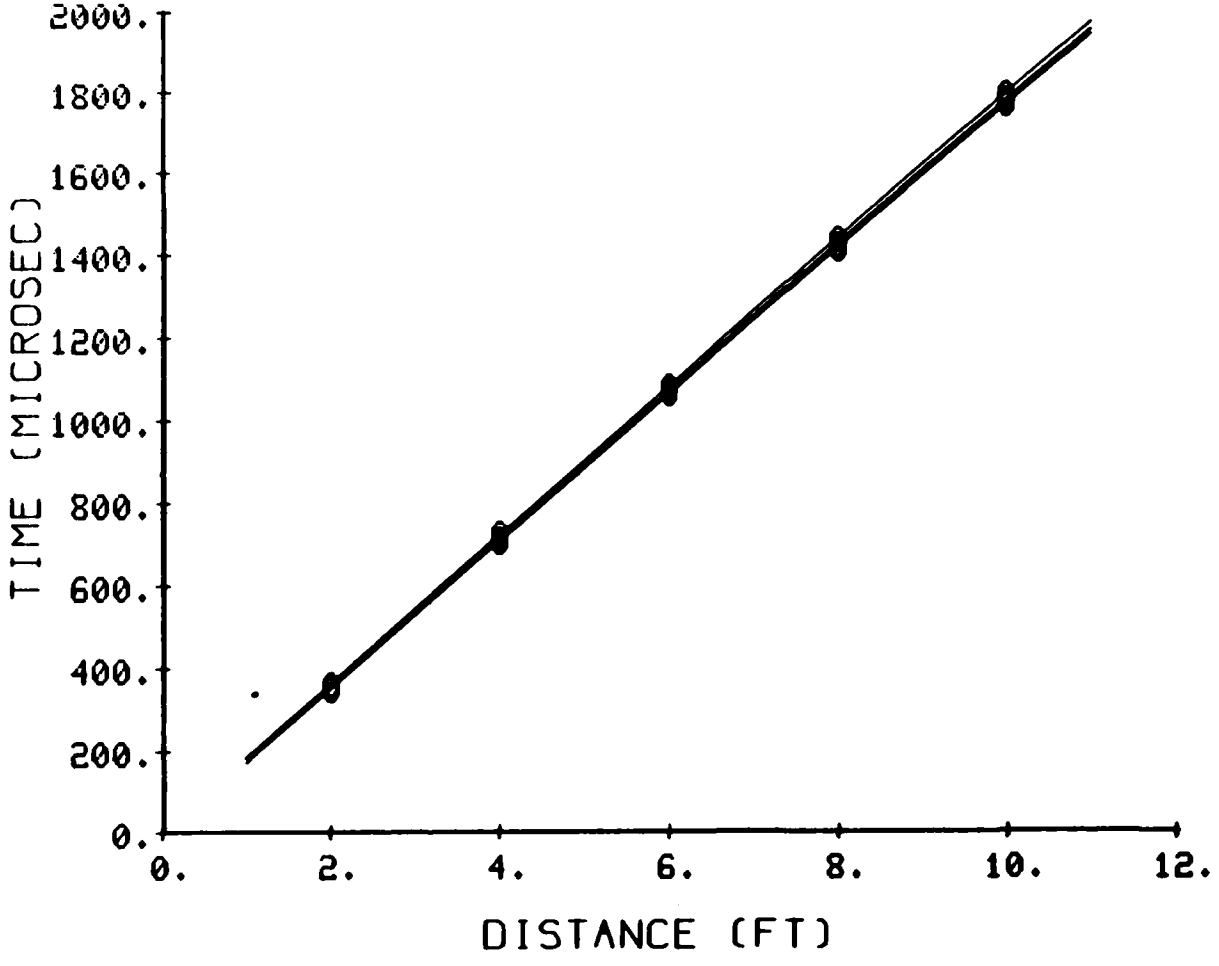

Figure 11. Time-Distance Trajectories, RDX-A, 1300 gm/m^3, 88% Air, 12% O_2, Driver Pressure 119.3 psia.

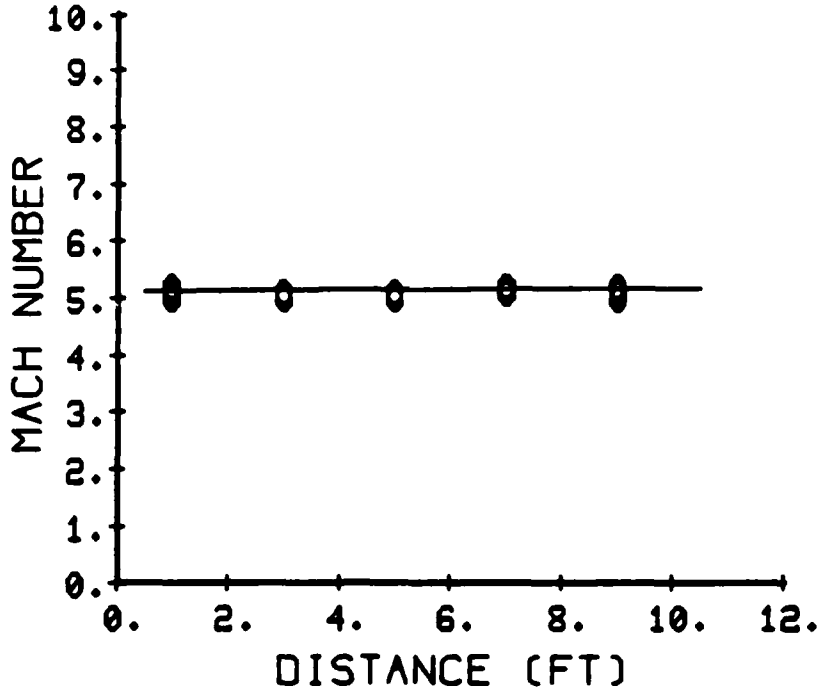

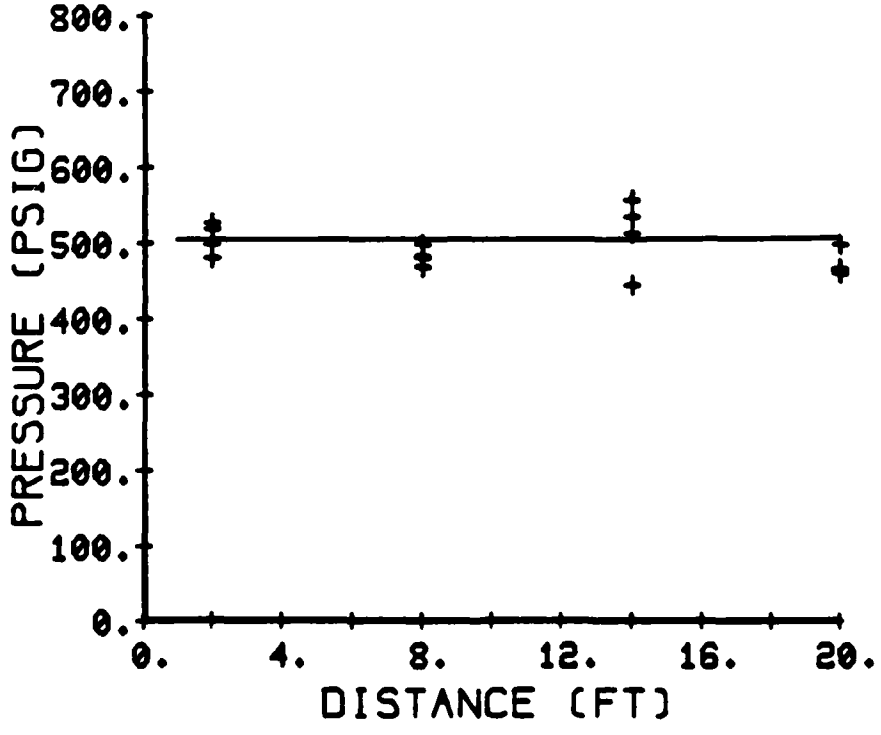

Figure 12. Wave Mach Number and Pressure RDX-A, 1300 gm/m^3, 88% Air, 12% O_2, Driver Pressure 119.3 psia.

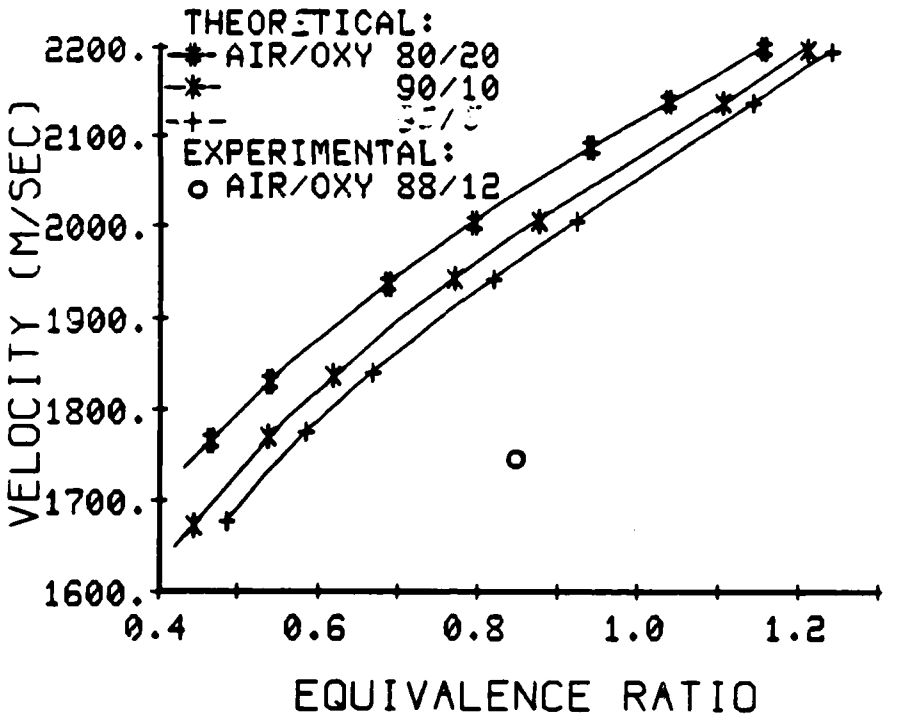

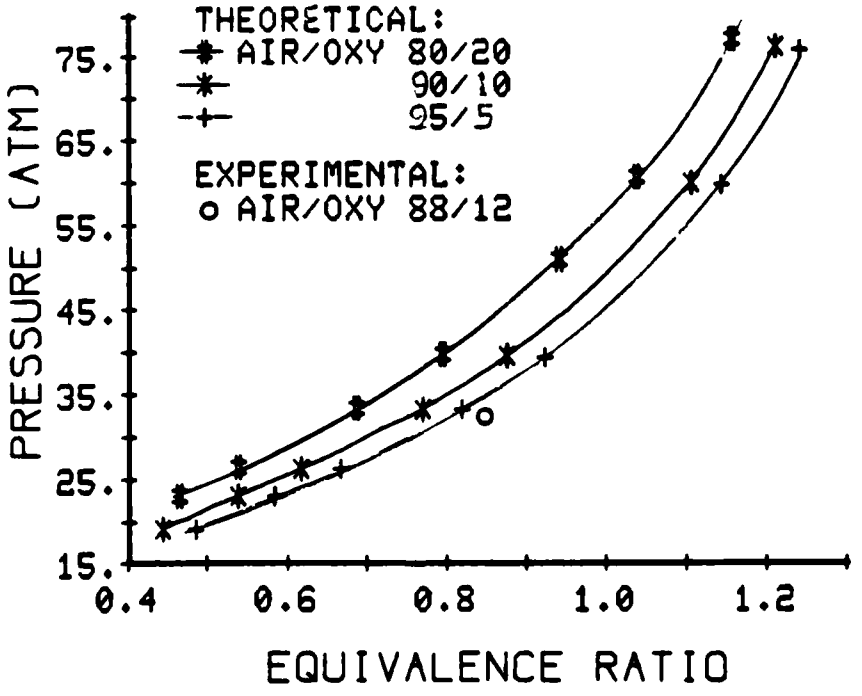

Figure 13. Computed and Measured Detonation Velocities and Pressures for RDX, 1300 gm/m^3.

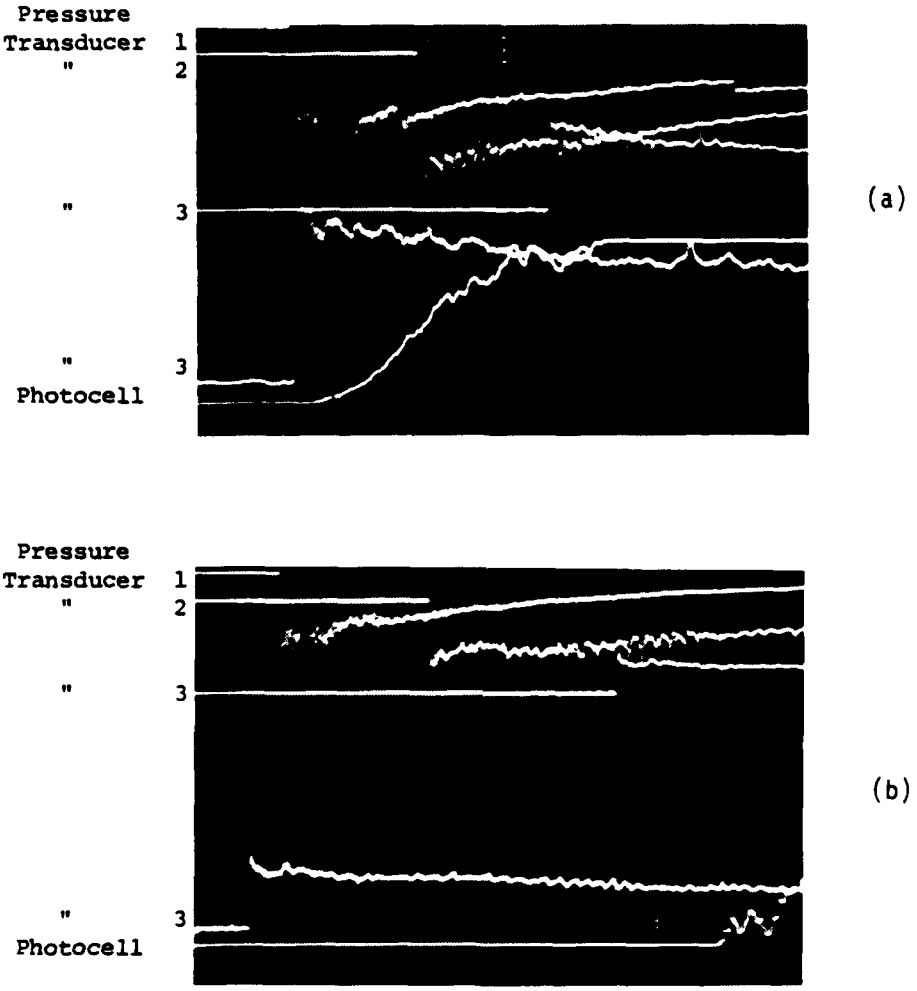

Figure 14. Light Emission and Pressure Records
Pressure Transducers 1, 2, and 3, respectively, 0.5 msec/div. Pressure Transducer 3 and the Photocell at the same location, 0.1 msec/div.

a) Detonation, Run #259, RDXA 1300 gm/m^3, 88% Air, 12% O_2, Driver Pressure 119.3 psia, 1/4 Driver.

b) Non-detonation, Run #272, RDXA 1300 gm/m^3, 100% N_2, Driver Pressure 119.3 psia, 1/4 Driver.

ignition occurs much later. Some streak photographs were taken for some of these same conditions and are shown in Fig. 15.

Reference to the detonation run in Fig. 15a shows that ignition occurs rapidly behind the shock wave (due to the high Mach number and temperature). From Fig. 15b it is noted that the flame in N_2 is weak and ignition occurs 1.8 msec after the incident shock wave. This is in agreement with the photocell output in Fig. 14b.

The photocell output in Fig. 16 shows the rise and fall of the flame light emission that indicates the combustion zone thickness. The same result was also derived from the streak photograph film strip, which shows that the flame lasts for approximately 3.5 msec.

RDX-E (smaller particles, 10 μm) were also tested under the same condition as RDX-A. However, in no case was detonation experienced. The waves were always decaying along the shock tube, as shown in Fig. 17. The oscilloscope output is shown in Fig. 18. Notice that the ignition delay (1.2 ms) is longer and the combustion zone is shorter (2 ms) than with RDX-A. This is an important point and is believed to be due to the inertia of the larger particle RDX-A, which has a mass of 15^3 times that of RDX-E. The larger particles lag the gas velocity for a much longer period of time behind the shock wave so that the particle experiences a higher stagnation temperature and the rate of heat transfer to the surface is higher. Thus, ignition occurs earlier. It is the induction zone, that lies between the lead shock wave and the ignition point, that has a substantial influence on the detonability of dusts.

3. Detonation of RDX/AP in Air

In the foregoing it was found necessary to use excess oxygen in order to achieve detonation. This fact suggested the possibility of furnishing the extra oxygen through the addition of an oxidizing dust. Accordingly, further detonation tests were made with the addition of AP, ammonium perchlorate (NH_4ClO_4), to the RDX dust. The results to be presented are expressed in terms of equivalence ratio and the make-up of the oxidizer, expressed as mass of air to mass of AP. Calculations relative to this are graphed

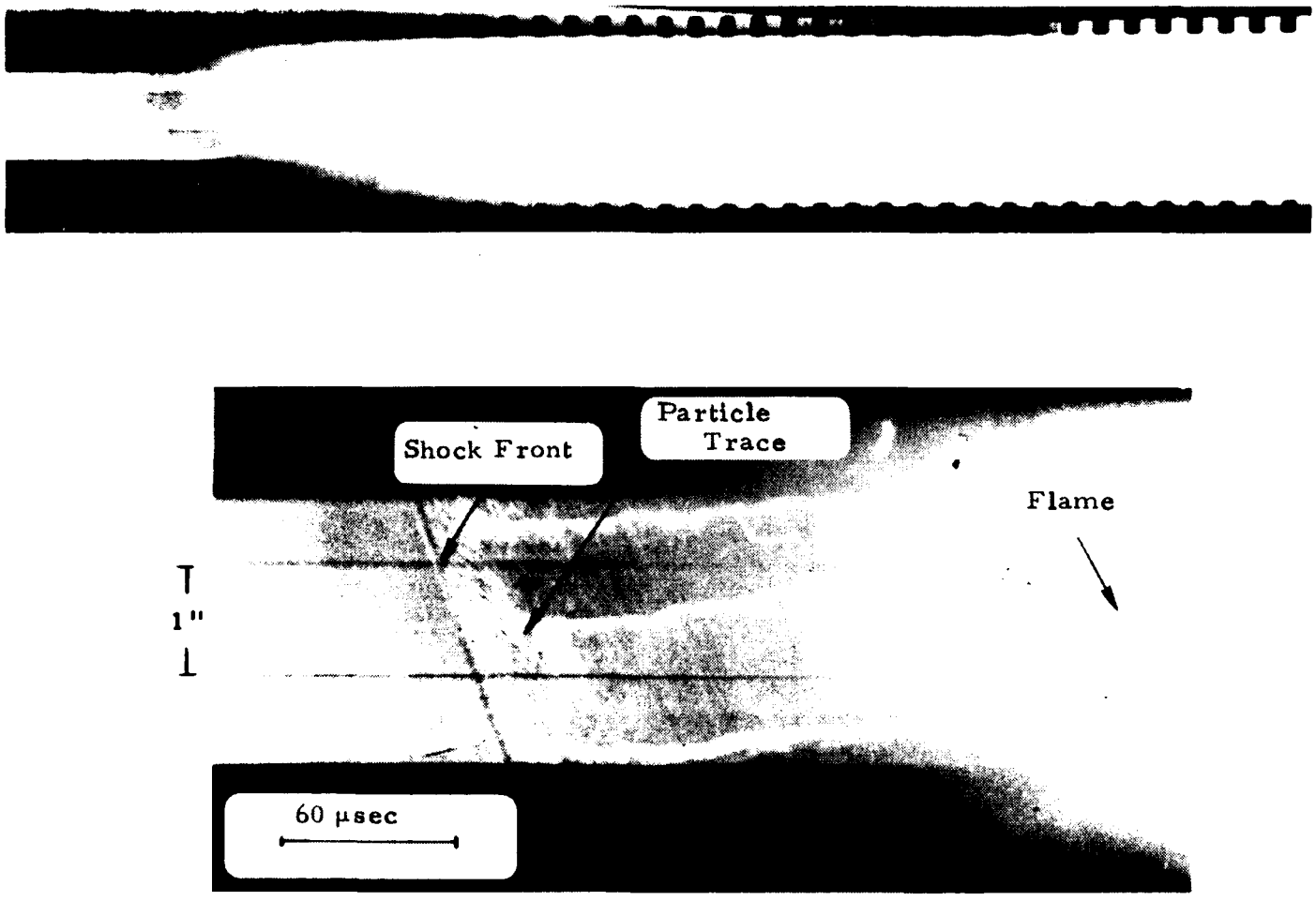

Figure 15a. Streak Schlieren Photograph of RDX-A (1300 gm/m^3) detonation in Air/Oxygen (88/12).

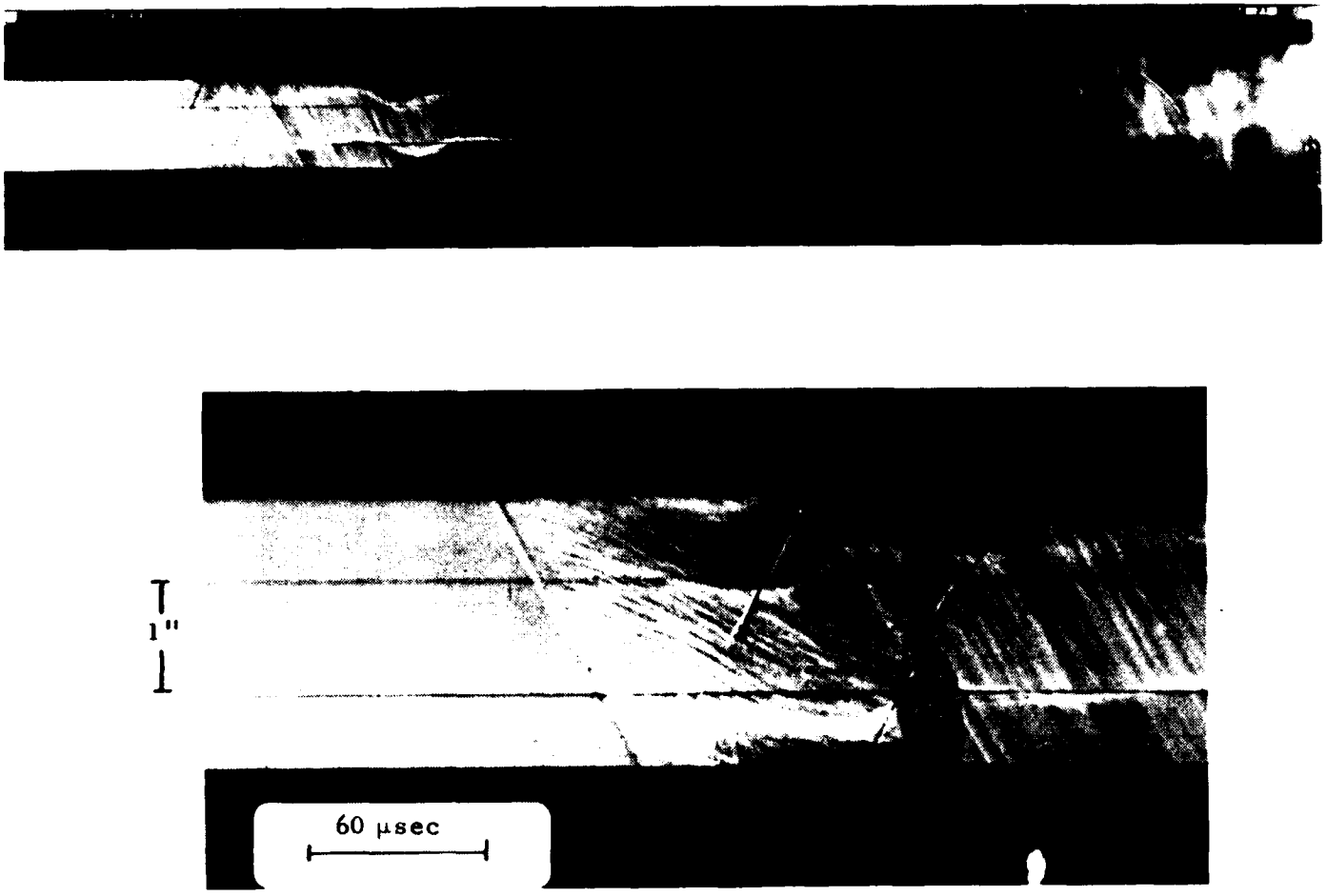

Figure 15b. Streak Schlieren Photograph of RDX-a (1300 gm/m^3) in Pure N_2 .

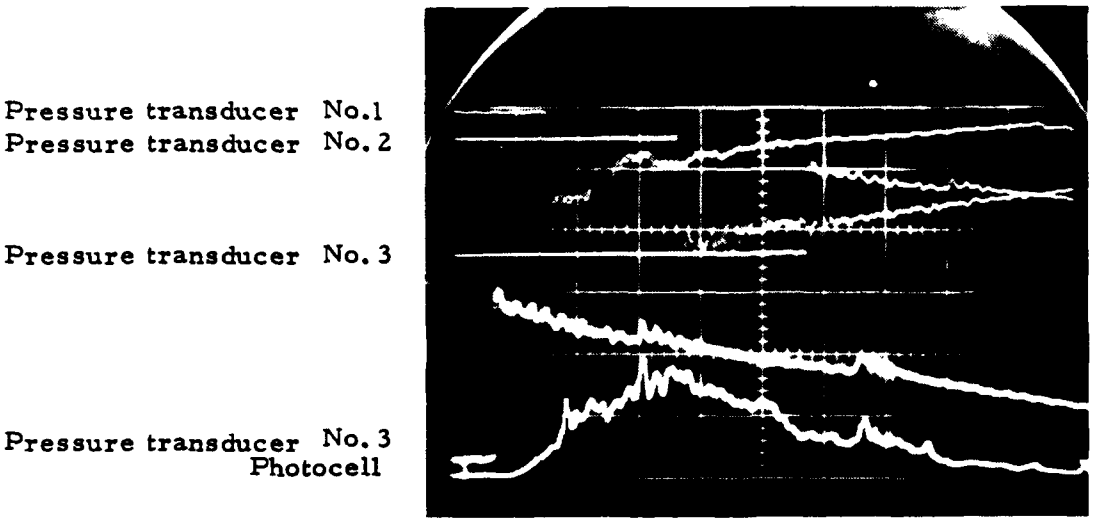

Figure 16. Light Emission and Pressure Records 0.5 msec/ div. for All Traces RDX-A 1300 gm/m^3, 88% Air, 12% O_2, Driver Pressure 119.3 psia.

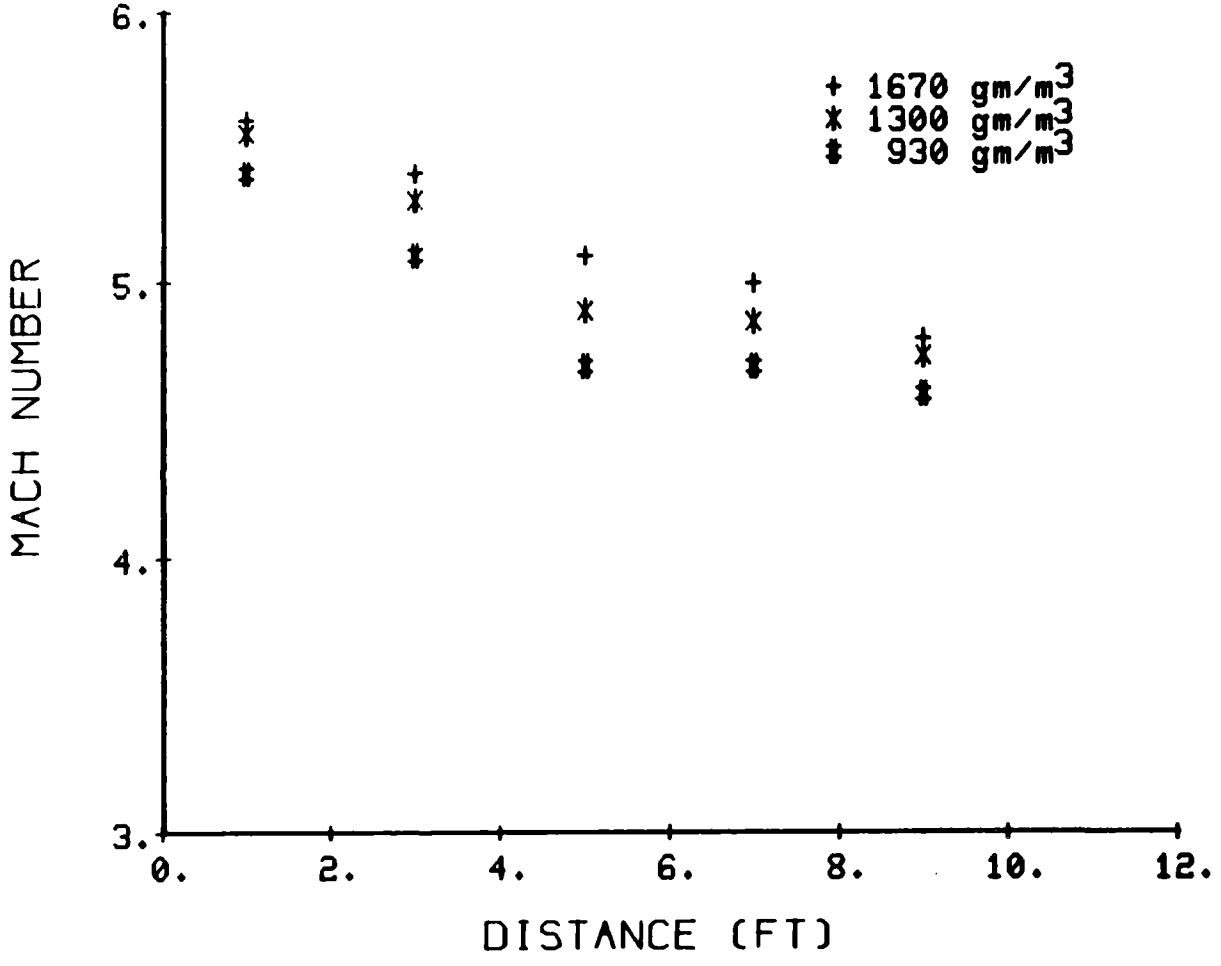

Figure 17. Wave Mach Number, RDX-E, 88% Air, 12% O_2, Driver Pressure 119.3 psia.

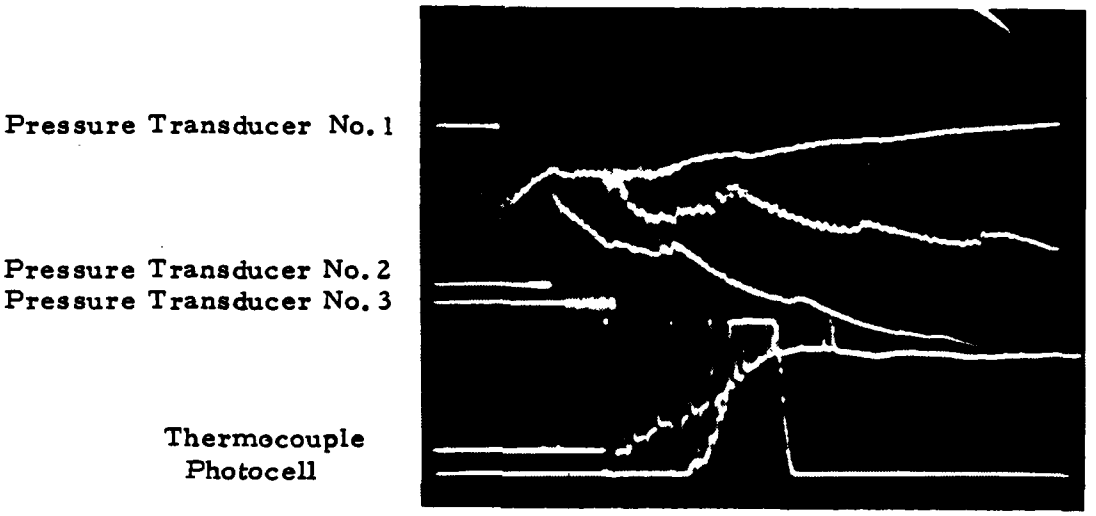

Figure 18. Light Emission and Pressure Records 0.5 msec/div. for All Traces RDX-E 1300 gm/m^3, 88% Air, 12% O_2, Driver Pressure 119.3 psia.

in Fig. 19. Figure 19a shows the variation of fuel/oxidizer ratio with equivalence ratio with concentration of RDX. The ratio of air to AP is a parameter in both cases. The equivalence ratio is that given by the computer program of Gordon-McBride [1]. From Fig. 19 it is seen that at higher dust densities (above 500 gm/m^3), AP plays the role of oxidizer, therefore, the larger the fraction of AP, the lower the equivalence ratio. However, at lower RDX densities AP behaves more as a fuel than as an oxidizer; therefore, the larger the fraction of AP, the higher the equivalence ratio. The computer output for the products of reaction showed that at low dust densities, a mild increase of AP would result in a significant increase of products such as ClO, H_2O and NO.

RDX-A/AP mixtures were tested at a driver pressure of 105 psig and detonation was achieved for ϕ = 0.88 and 0.84. Some Mach number and pressure ratio results are shown in Figs. 20a and 20b. Near the end of the shock tube, where it appears to be a steady detonation, the Mach numbers and pressure ratios are approximately 4.9 and 32 for ϕ = .84 and 5.0 and 34 for ϕ = 0.88 respectively. The Mach number plots indicate that initially the wave is overdriven and then decays to a stable detonation wave upon propagating further downstream. The data for the ϕ = .84 runs show a slight minimum in Mach number followed by acceleration of the wave. This characteristic is well known for blast wave initiated detonations. A comparison of experimental and theoretical results is shown in Fig. 21. The experimental values are approximately 13% and 15% lower than theoretical for detonation velocity and pressure respectively. In general, it was found that the addition of AP to air did encourage detonation but, on the other hand, the oxygen was not as readily available as in the case of gaseous oxygen.

A number of runs were made with RDX-E (the smaller particles) mixed with AP. Several equivalence ratios were tested but, as in the earlier tests, no detonation was observed.

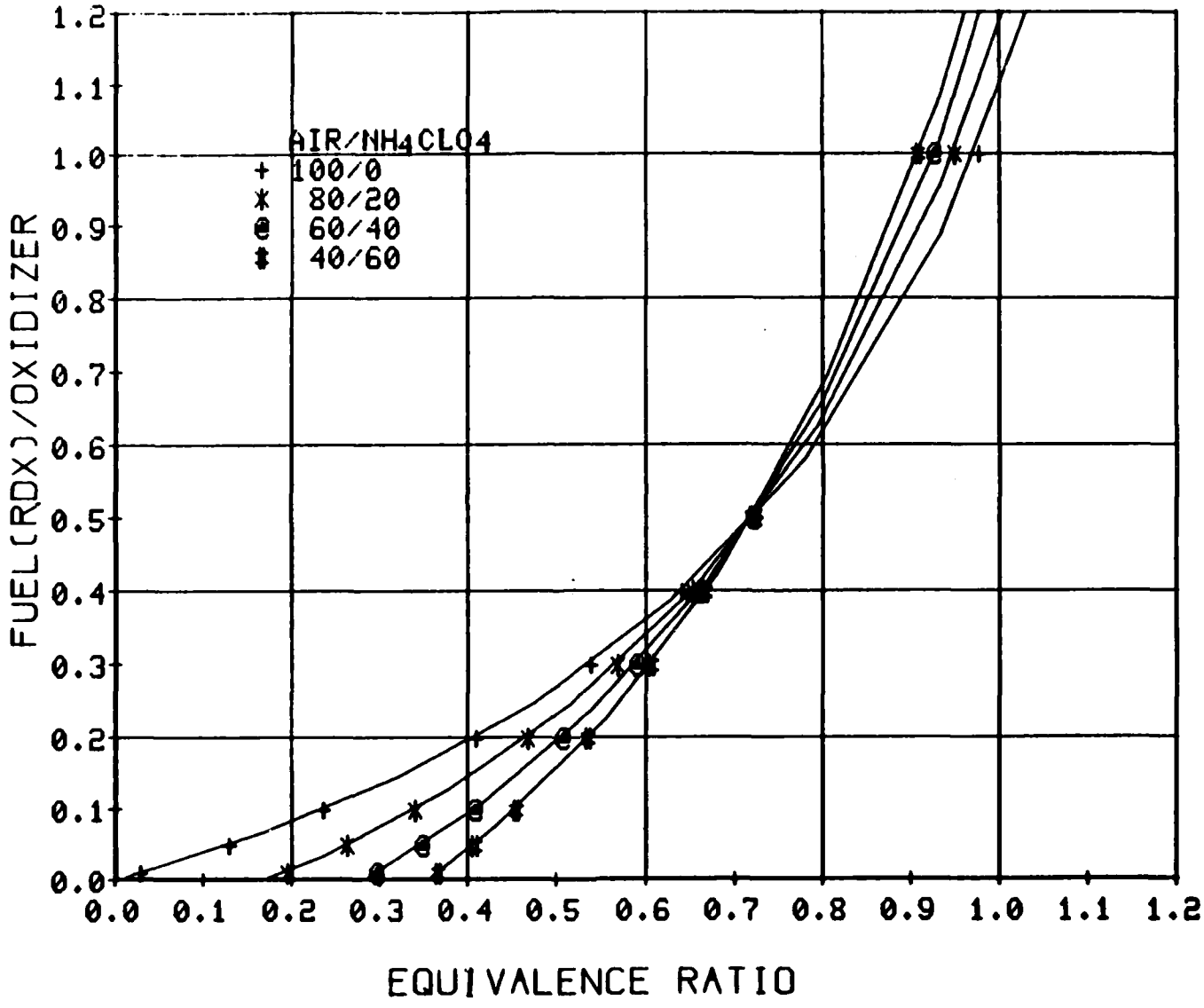

Figure 19a. Fuel/Oxidizer Ratio Versus Equivalence Ratio.

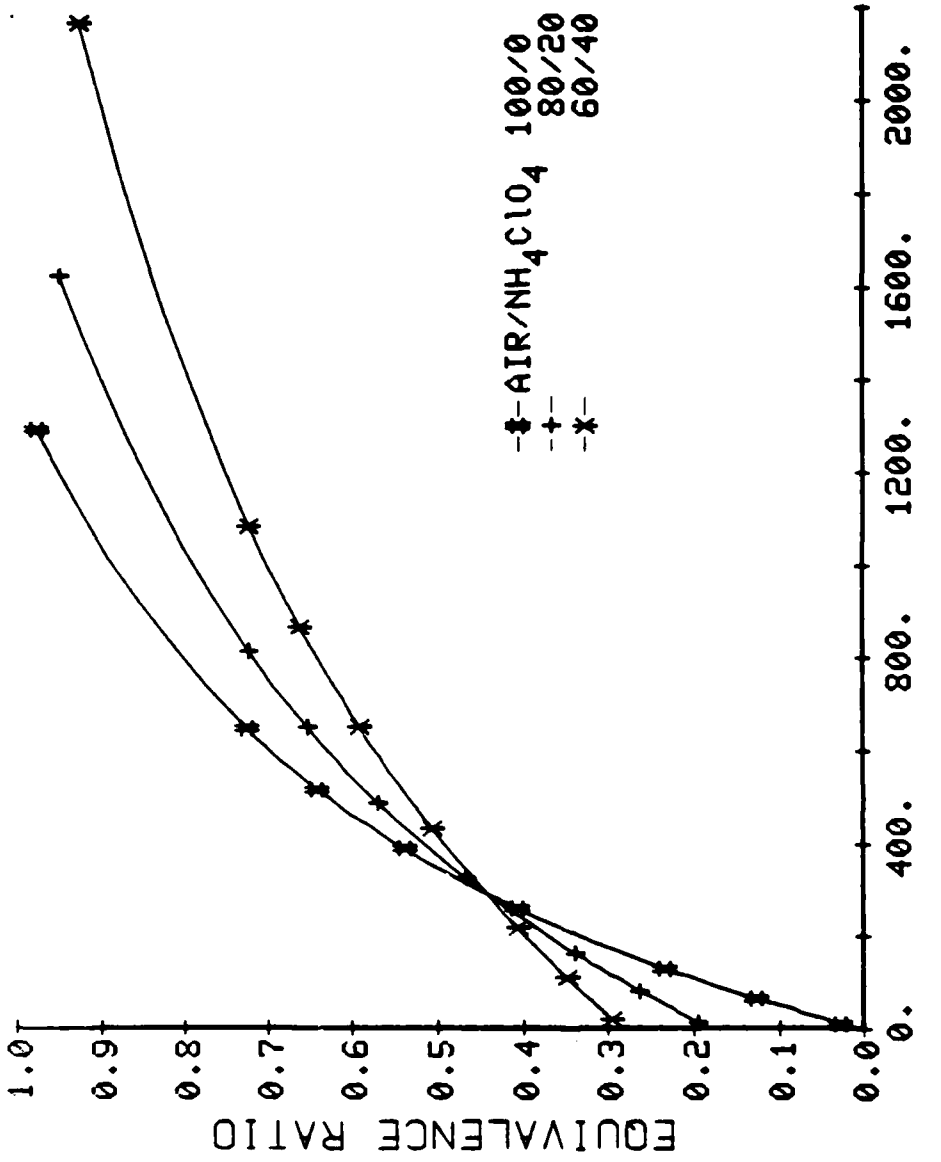

Figure 19b. Dust Density Versus Equivalence Ratio.

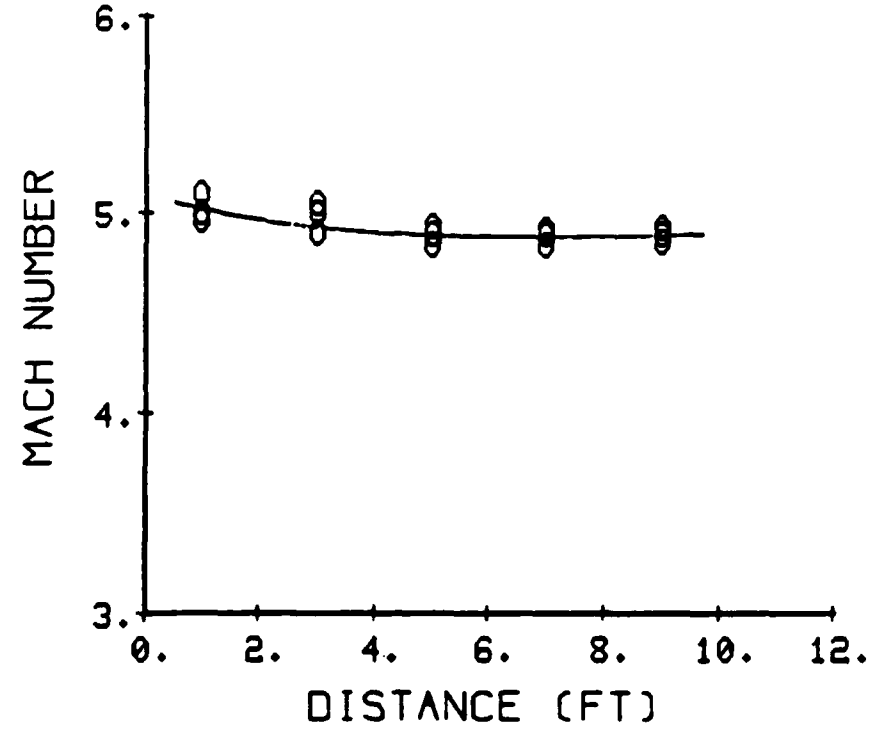

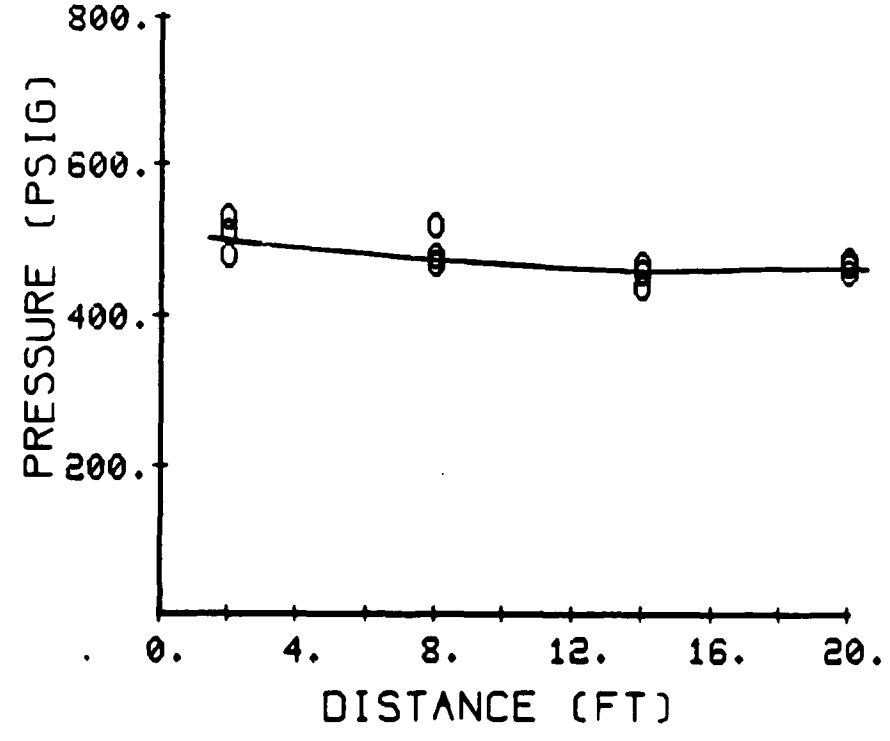

Figure 20a. Wave Mach Number and Pressure, 83%, RDX-A + 17% Ammonium Perchlorate, 100% Air, 1340 gm/m^3, ϕ = .84, Driver Pressure 119.3 psia.

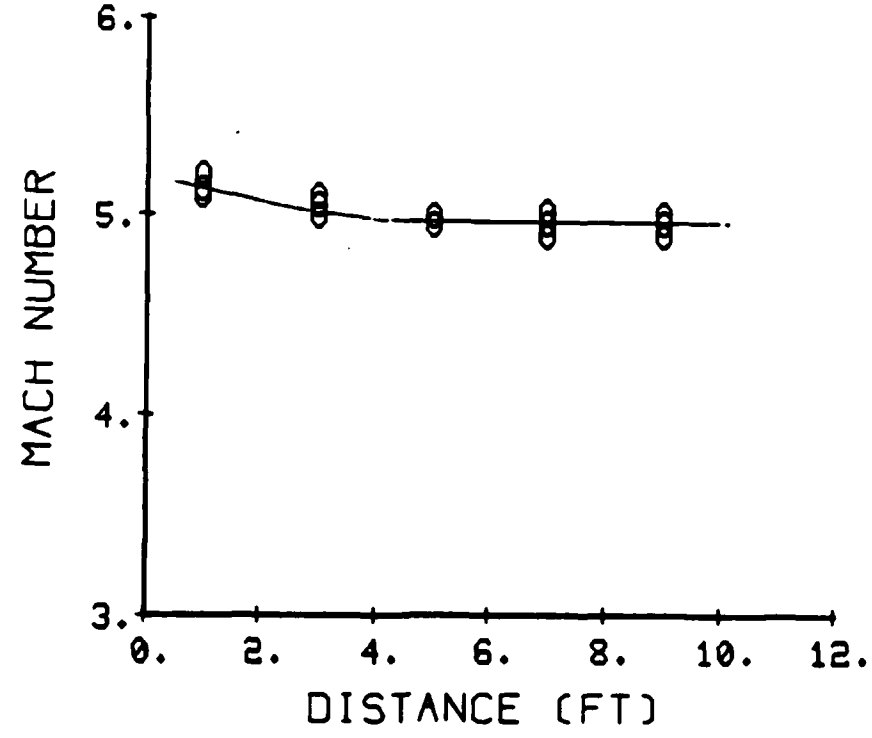

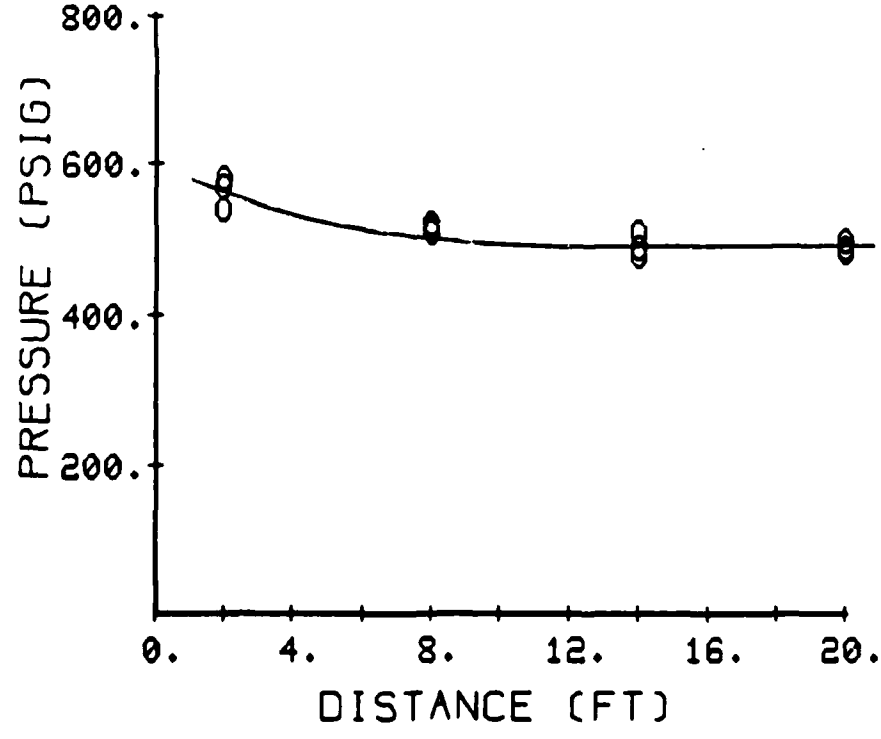

Figure 20b. Wave Mach Number and Pressure, 83% RDX-A + 17% Ammonium Perchlorate, 100% Air, 1500 gm/m^3, ϕ = .88, Driver Pressure 119.3 psia.

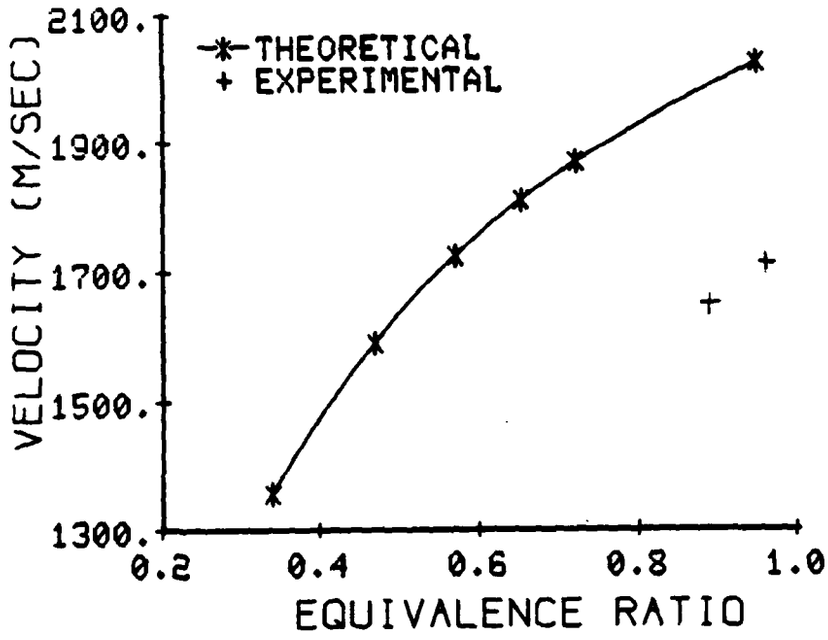

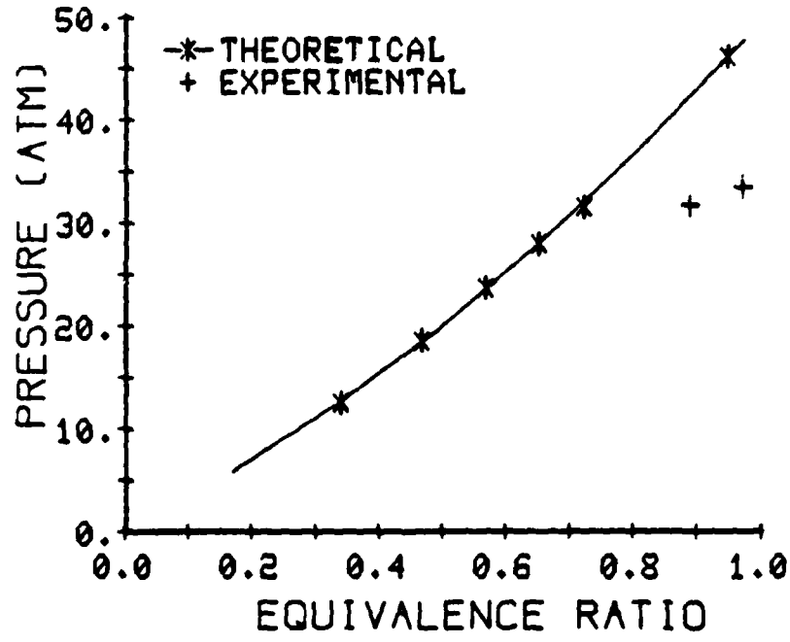

Figure 21. Computed and Measured Detonation Velocities and Pressures for RDX-A/AP (83/17) in Air.

4. Detonation of Aged RDX

The RDX dust was retested eleven months after the above tests were completed, which was 20 months after the arrival of the dust. The retested results remained the same for RDX-A. However, there were significant changes for RDX-E. The latest tests of RDX-E showed a higher wave Mach number (7.0) and pressure ratio (50) whereas the earlier runs of new RDX-E dust reached a wave Mach number of 4.8 and pressure ratio of 2.2 near the end of the shock tube. Figure 22 shows the time-distance trajectories of some of the new and old RDX-E dust runs. The dried dust showed a faster but decaying wave pattern whereas the undried dust showed a slower but steadier or somewhat accelerating wave pattern. None of them had achieved C-J condition. It appeared that these waves were undergoing a transition period. The streak schlieren photograph is shown in Fig. 23a. It is interesting to notice that the ignition delay or induction zone is hardly visible and combustion occurred almost immediately behind the shock wave. Further behind the shock wave, some wave patterns seem to be moving faster than and toward the front shock wave. The mechanism of this peculiar phenomenon is not well understood . It is suspected that chemical and physical changes as well as the decay of plastic coating may have occurred to the RDX dust after a long storage period. Electron micrographs of the aged dust were taken and are shown in Fig. 23b. A definite difference can be seen. The surface of the aged dust appears to be more rough, presumably due to the decay of the plastic coating.

5. Ignition of Liquid/ Dust Drops

An interesting variation of a dust detonation, which could be called a three-phase detonation, is that wherein a combustible dust is mixed with a liquid fuel. The detonation of this combination in a gaseous oxidizer could be called a three-phase detonation. In recognition of the fact that the

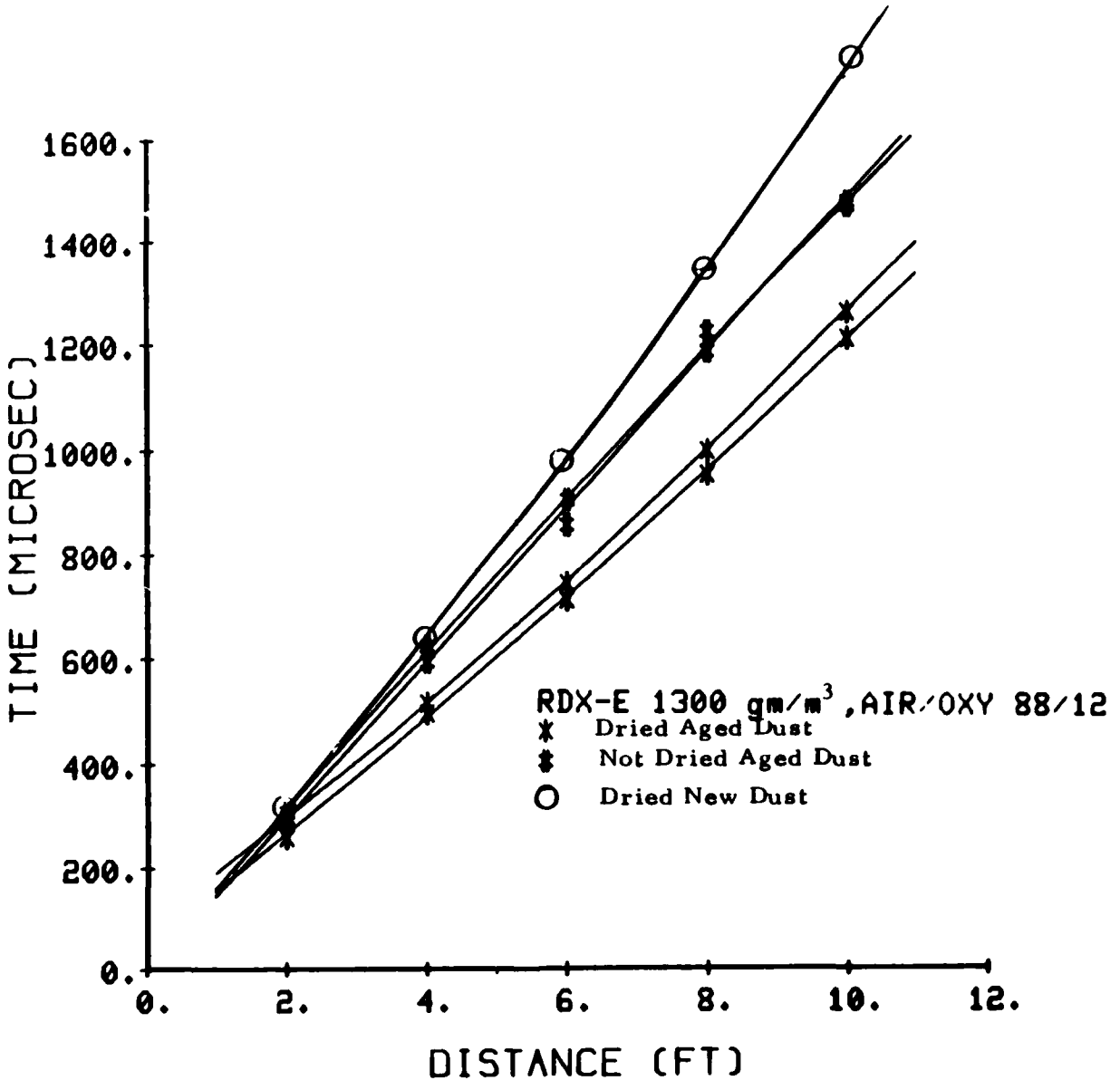

Figure 22. Time-Distance Trajectories of RDX-E, 1300 gm/m^3, 88% Air, 12% O_2, Driver Pressure 119.3 psia.

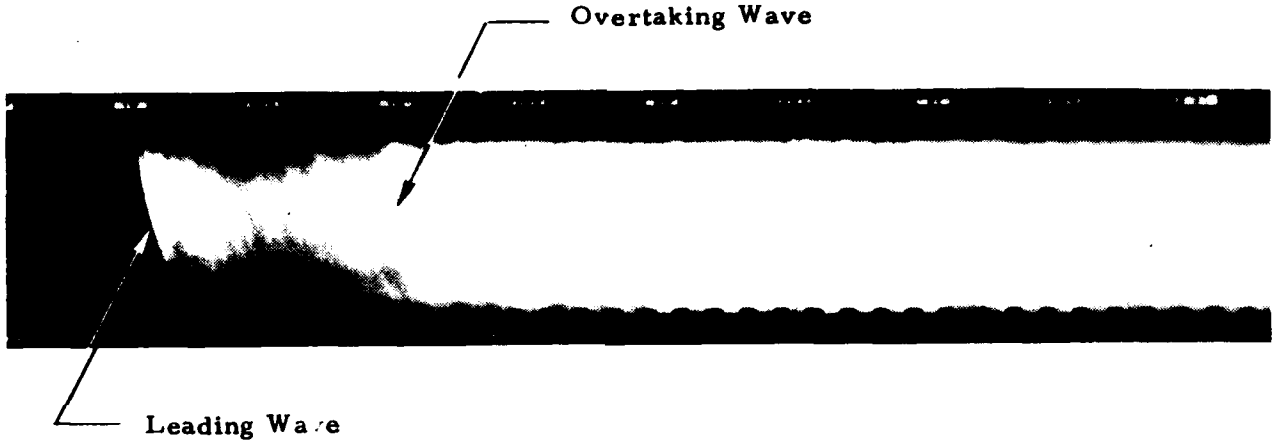

Figure 23a. Streak Schlieren of Aged RDX-E, 1300 gm/m^3, 88% Air, 12% O_2, Driver Pressure 119.3 psia.

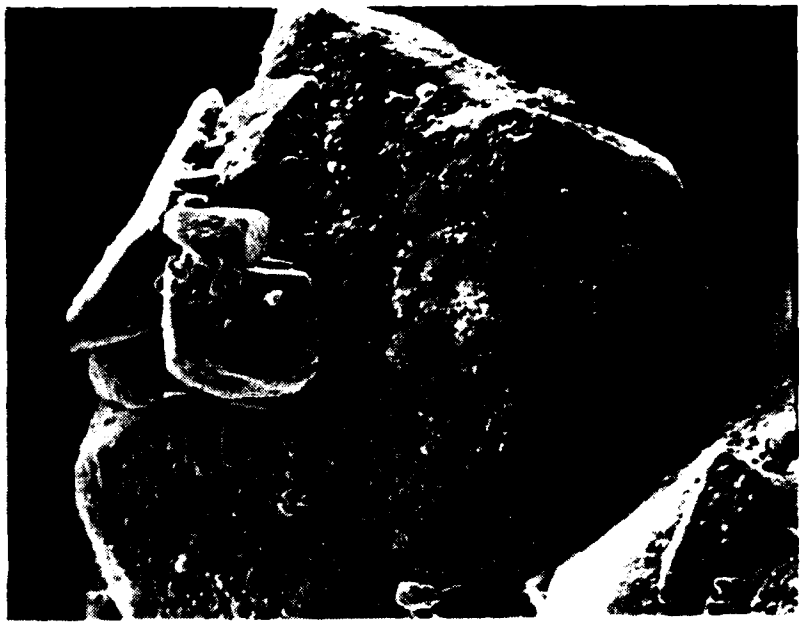

(a) New Dust

(b) Aged Dust

Figure 23b. Electron, Micrographs of RDX Particle 400 X.

shock wave ignition process is a key part of such a heterogeneous detonation, an experimental effort was initiated on that facet.

For these studies a single droplet was suspended on a needle in the test section. The driven section of the tube was filled with oxygen and the driver gas was helium. Rupture of the diaphragm allowed a strong shock wave to propagate through the driver section and over the drop. The resultant interaction was monitored by streak photography.

Various dusts were mixed with liquid decane; these included RDX-E, AP, and Al_2O_3. In all the dust liquid mixtures, a small amount (3-5% by weight of the decane) of cabosil (SiO_2) was added, which helped to achieve a homogeneous dust particle suspension in the liquid drops and to increase the viscosity and surface tension of the droplets. Streak schlieren photographs were taken to investigate the droplet shattering and ignition processes. Some typical results are shown in Fig. 24. Figure 24a is a decane droplet and Fig. 24b is an RDX/decane droplet, consisting of 40/60 (by weight) mixture of RDX-E and decane, respectively. Each droplet is 3000 μm in diameter and exposed to a shock wave of M = 3.5 in one atm.of oxygen. Both photographs show similar structures. The aerodynamic force on the droplet behind the shock wave causes the droplet to break up. The breakup process is mainly determined by the surface tension and size of the droplet as well as the dynamic pressure behind the shock wave and is mildly influenced by the viscosity of the droplet. Following the breakup, a wake (indicated by the growth of the dark region) is formed behind the drop. The acceleration of the disintegrating droplet in the shocked gas flow is indicated by the curvature of the droplet's leading edge trajectory. A bow shock is formed in front of the leading edge. After a delay of T_{ig}, ignition (indicated by the bright burst of flame) occurs in the wake region and the flame rapidly propagates upstream toward the leading edge of the drop. The ignition delay T_{ig}, and the flame speed are estimated to be 85 μsec and 1700 m/sec for the RDX/decane droplet. These high flame speeds indicate that these fronts are really blast waves driven by combustion. The ignition delays are relatively long as compared

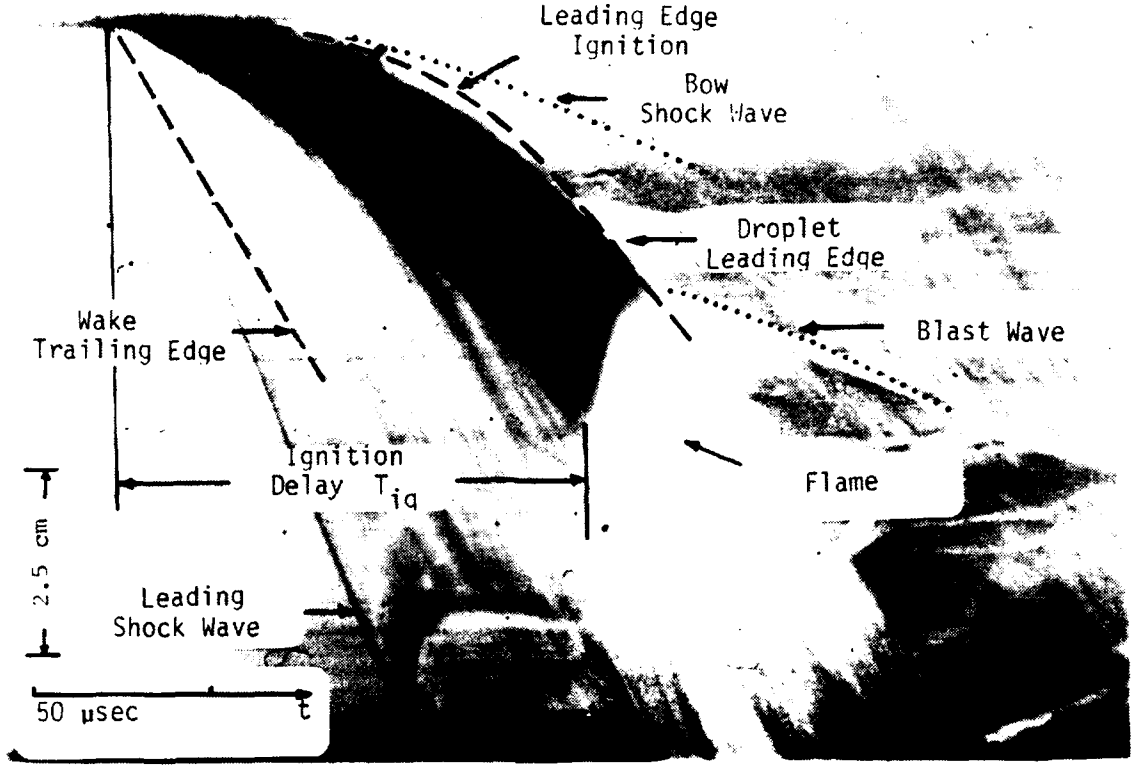

Figure 24a. Run #501, Decane/Cabosil Droplet, 3000 µm, M = 3.5.

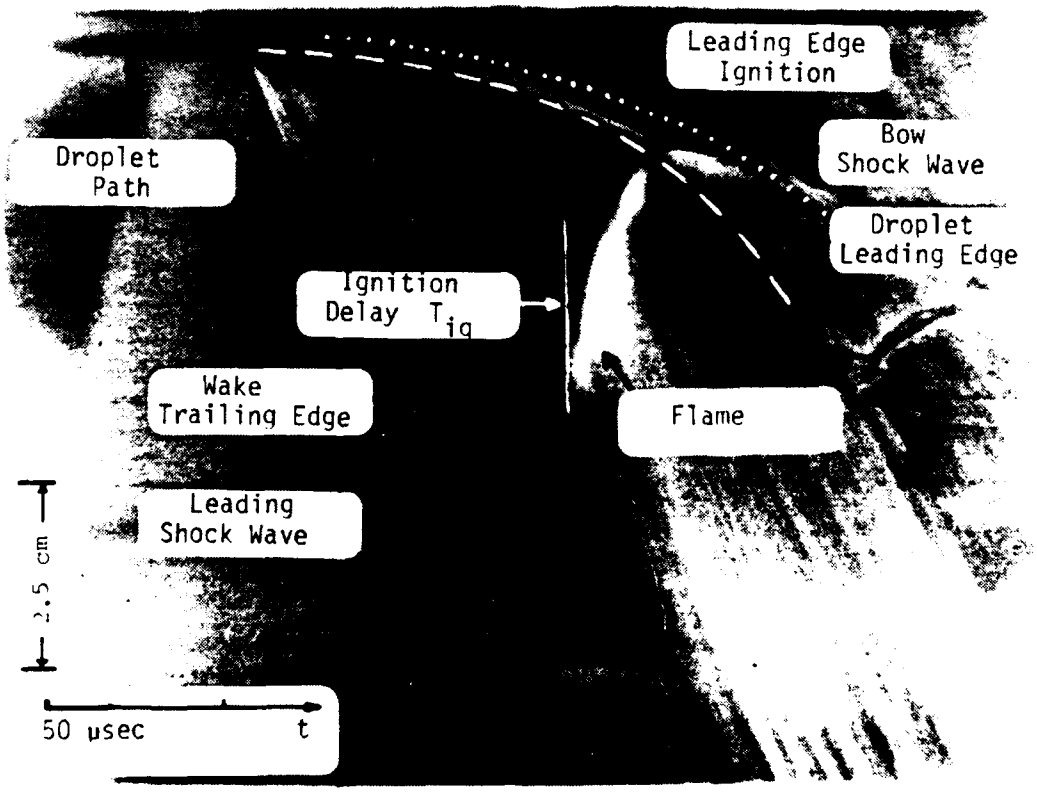

Figure 24b. Run #502, RDX-E/Decane/Cabosil Droplet, 3000 µm, M = 3.5.

to most heterogeneous detonations. However, the shock wave Mach number of 3.5 is low compared to most detonation Mach numbers. The stagnation temperature behind the bow shock wave is 1300 K for an incident shock wave of M = 3.5. It appears that this high temperature causes some chemical reaction at the leading edge of the drop just behind the bow shock wave. The luminosity, observable in both photographs, is less distinct than the main ignition in the wake region. It is to be noted that the wake ignition occurs significantly sooner when the dust is present.

The experimental runs were divided into several groups, depending on the droplet size and dust content. The test results were compared with each other and are reported in the following order:

1. 2000 μm droplets
   a. decane
   b. decane/ RDX
2. 3000 μm droplets
   a. decane
   b. decane/ RDX
   c. decane/ RDX/ AP
   d. decane/ Al_2O_3

1. 2000 μm Droplets

a) Decane

The ignition tests of 2000 μm decane droplets are shown in Fig. 25. The well defined burst type of ignition shown in Figure 24 was hardly observed for the 2000 μm decane droplet case. However, the streak schlieren photographs show that combustion does occur at the leading edge of the droplet, as well as in the wake for sufficiently high Mach number. At the higher Mach numbers, the faster disintegration and combustion of the droplet are indicated by the quicker disappearance of the dark area, which is the microspray.

b) Decane/ RDX

The ignition tests of 2000 μm decane/ RDX (60/40) droplets are shown in Fig. 26. By comparison with pure decane, Fig. 25, the breakup,

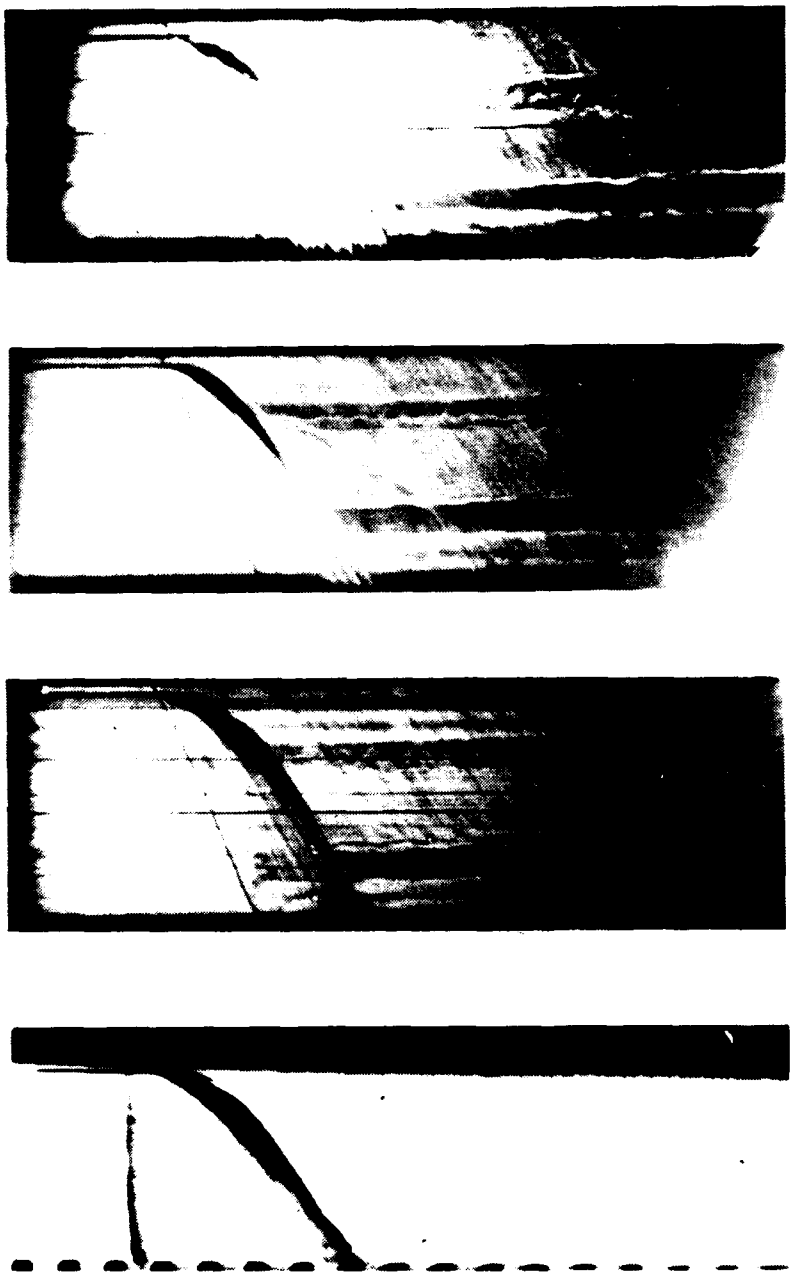

Figure 25. Ignition of 2000μm Decane Droplet

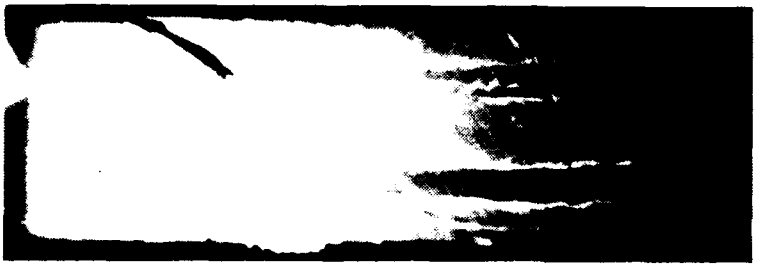

M = 3.84

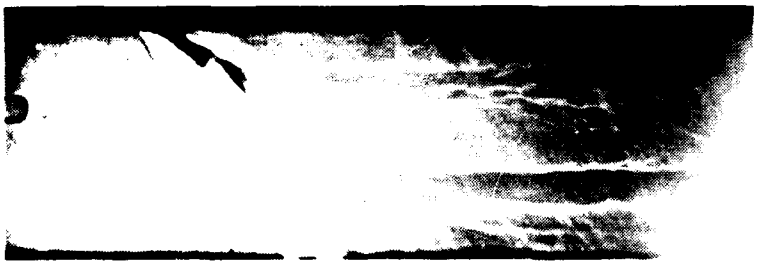

M = 3.77

M = 3.69

M = 3.57

Figure 26. Ignition of 2000 μm Decane/ RDX (60/40) Droplet.

acceleration and displacement of these two kinds of droplet are quite similar. However, the effect of the RDX additive is to produce the burst type of flames ignited in the wake region. The higher the Mach number, the shorter the ignition delay. At higher Mach numbers, the luminosity at the leading edge of the droplet is greater because of the higher stagnation temperature and consequent ignition.

2. 3000 μm Droplets

a) Decane

Unlike the 2000 μm decane droplets, the 3000 μm decane droplets showed clear ignition in the wake region for many of the runs (Fig. 27). Compared with the 2000 μm droplet, the larger droplet showed a wider wake and slower acceleration, and is similar to the 2000 μm decane/RDX droplet in that higher Mach number resulted in earlier combustion without the distinctive wake explosion.

b) Decane/RDX

The decane/RDX droplets were tested at various RDX contents, 80/20, 60/40, and 50/50 in mass ratios. It is interesting to compare the ignition delays of 2000 μm and 3000 μm decane/RDX (60/40) droplets as shown in Figs. 26 and 28. The larger droplets showed smaller ignition delays, which is surprising. Generally, in shock wave droplet ignition where no dust is present, the aerodynamic breakup time of the droplet is nearly proportional to the droplet diameter and the longer the breakup time the longer the ignition delay. Ignition usually occurs in the wake region where the microspray which was formed has mixed with the oxidizing gas. The mechanism of three phase ignition, which evidently differs from the two-phase case, may be strongly affected by the presence of the explosive RDX dust in the decane microspray. Thus, it may be the RDX instead of the decane that dominates the ignition. Now the larger drops (3000 μm) breakup and accelerate at a lower rate than smaller drops and hence are exposed to a hotter surrounding gas for a longer period of time. Therefore,

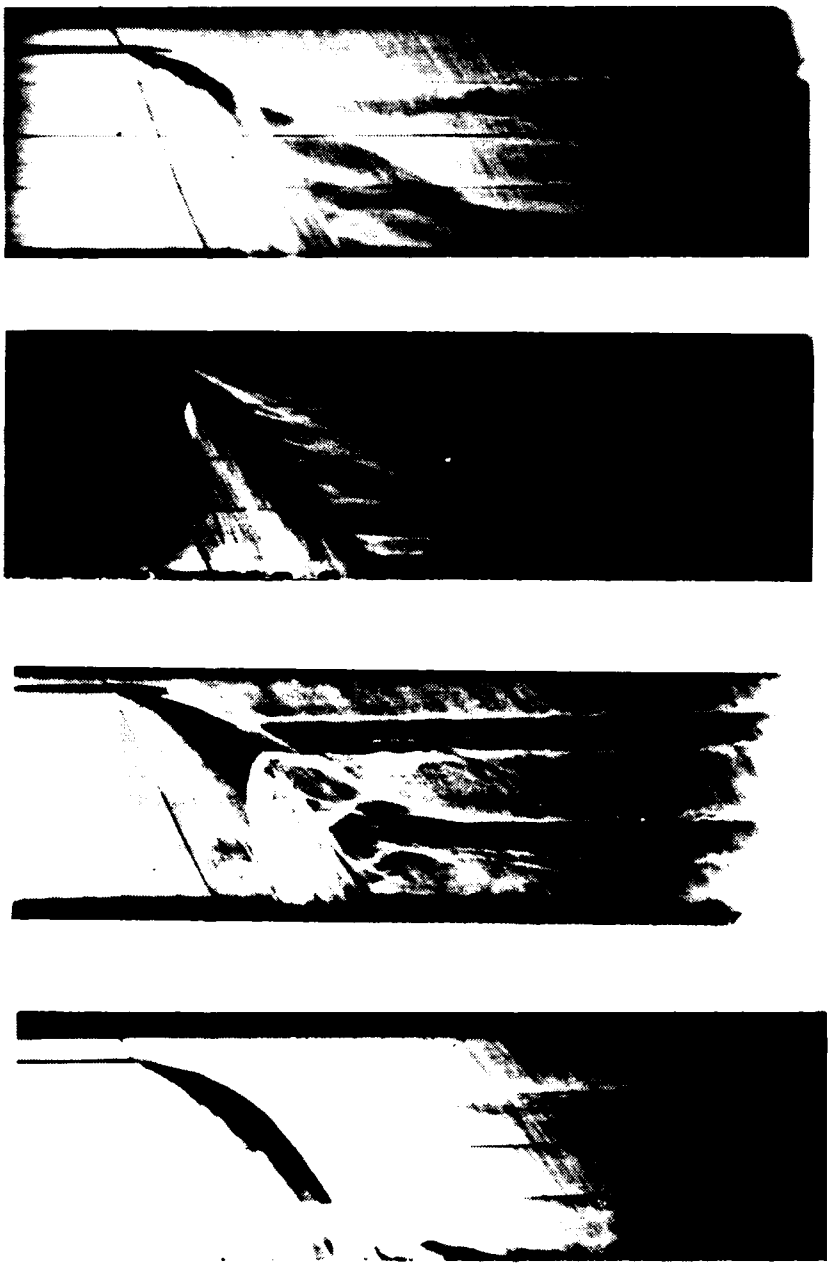

Figure 27. Ignition of 3000 μm Decane Droplet.

M = 3.85

M = 3.68

M = 3.55

M = 3.44

Figure 28a. Ignition of 3000 μm Decane/ RDX (60/40) Droplet.

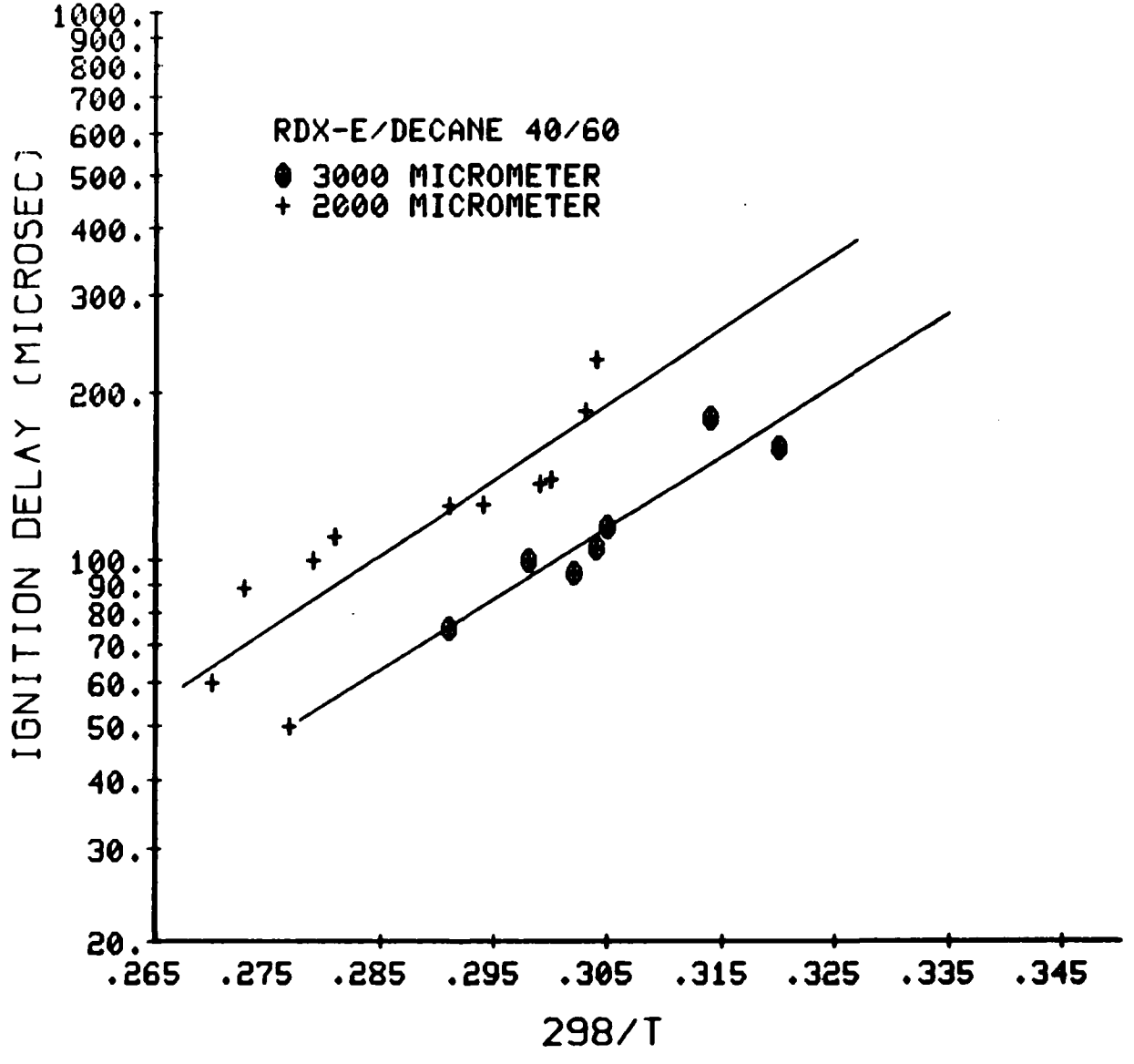

Figure 28b. Ignition Delay of RDX-E/ Decare Droplets in Various Sizes.

the larger drops with RDX content may absorb more heat and ignite earlier. This is a similar mechanism to that encountered in RDX dust detonation tests wherein the larger particle RDX-A had shorter ignition delay.

The ignition delay versus reciprocal temperature (function of shock Mach number) for RDX/ decane droplets with various RDX content is shown in Fig. 29. It is apparent that the presence of RDX extends the range of ignition to lower values of temperature (or shock Mach number). Higher RDX concentration apparently lowers the ignition time delay at the lower temperatures but does not make much difference at the higher temperatures.

c) Decane/ RDX/ AP

In further tests, AP particles, of diameter less than 50 μm, were added to decane/ RDX in the mass ratio of 80/ 20/ 20. The comparison of decane/ RDX/ AP with decane and decane/ RDX is shown in Fig. 30. The addition of AP resulted in effects very similar to that for the addition of RDX to decane, but it added to the magnitude of the change. Presumably this would make such a mixture easier to detonate.

d) Decane/ Al_2O_3

Another facet of droplet ignition investigated was that wherein an inert dust was added to the liquid. Aluminum oxide, Al_2O_3, of size 80 μm and less, was chosen as the dust. Streak schlieren photographs for two different shock strengths are shown in Fig. 31. Figure 31a shows at least three successive ignitions; some of the attendant blast waves can also be observed. Figure 31b shows two or three ignition points, with the last being of low luminosity and identified by the blast wave due to the explosion of the unburned vapor trapped in the wake.

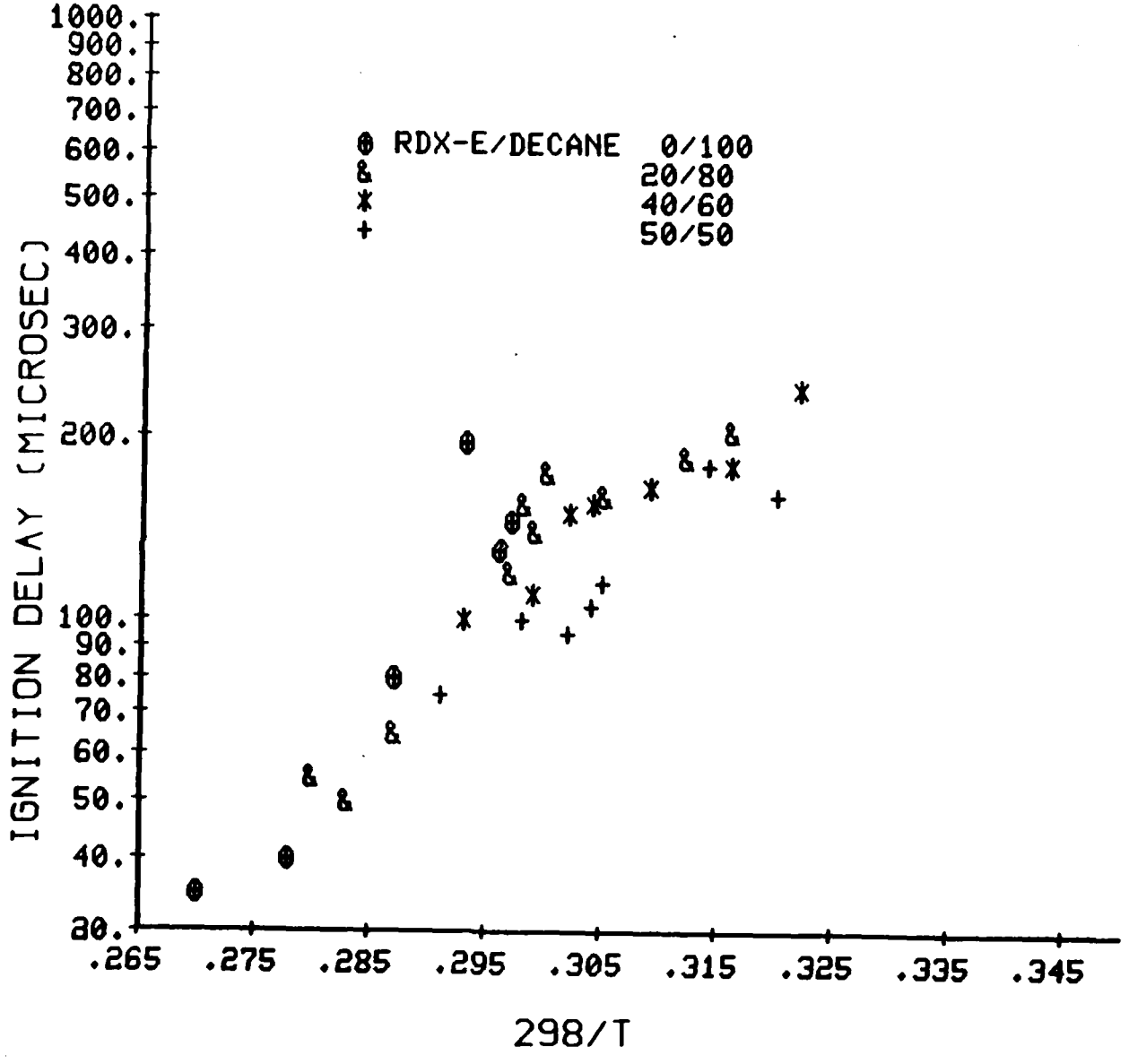

Figure 29. Ignition Delay of Some RDX-E/ Decane Droplets.

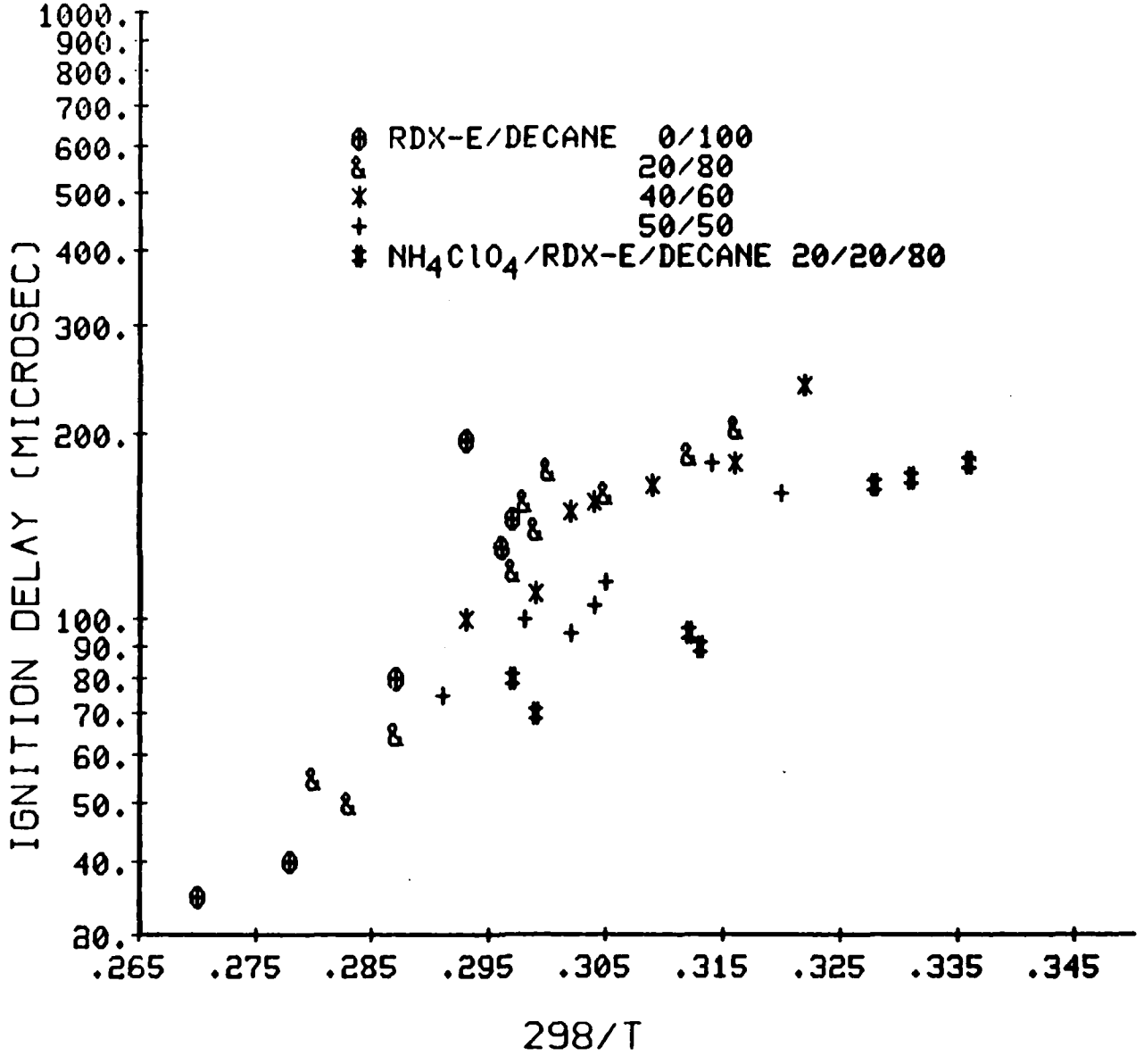

Figure 30. Ignition Delay of Some Droplets.

(a) M = 3.63

(b) M = 3.49

Figure 31. Ignition of Al_2O_3/ Decane (10/90) Droplet.

A comparison of the ignition delay of decane with decane/ Al_2O_3 is shown in Fig. 32. As seen, the inert appreciably reduces the delay time. A further comparison with the AP case is shown in Fig. 33. Evidently the inert dust yields shorter ignition delays at the higher temperatures but the AP can extend ignition to lower temperatures.

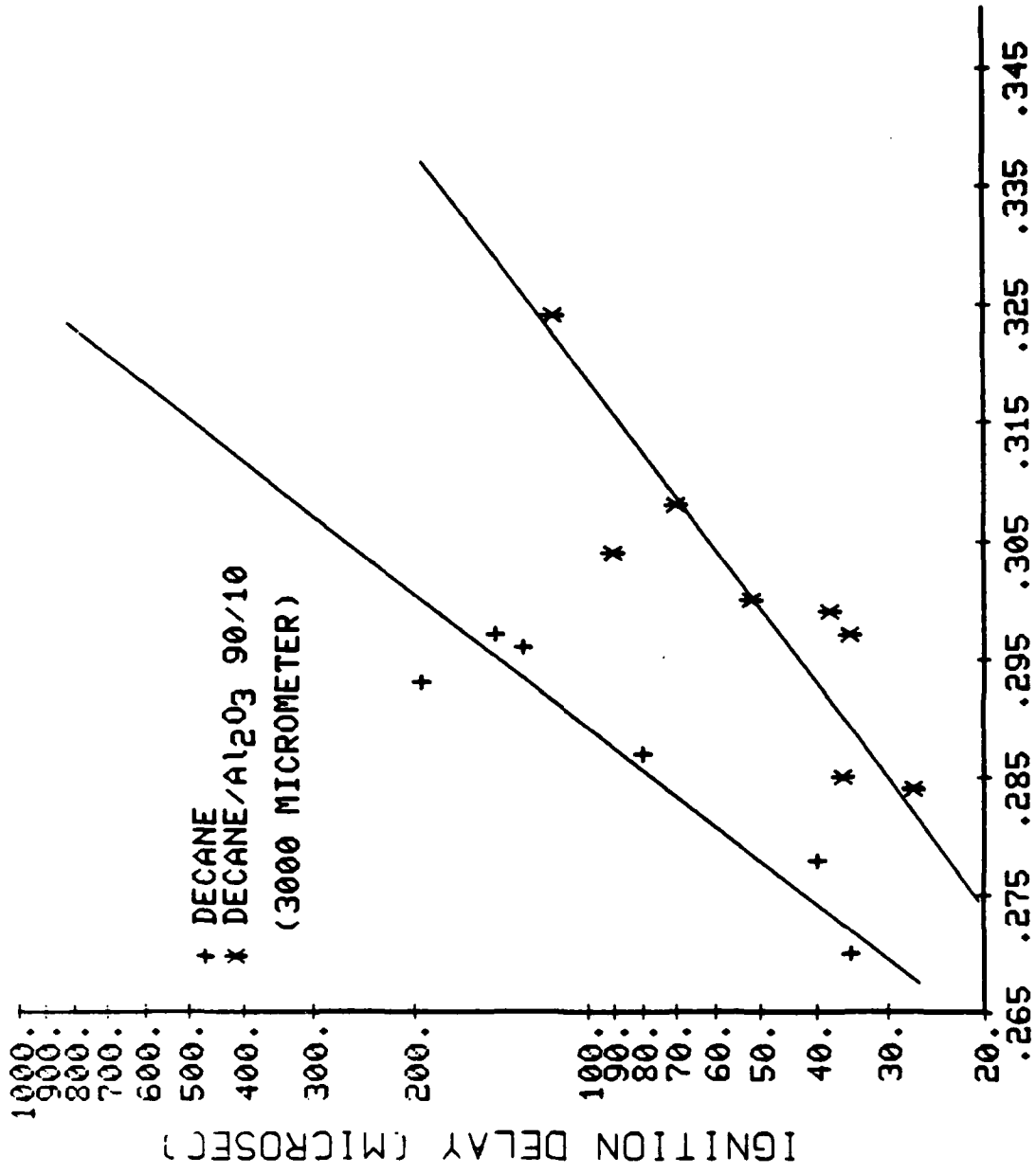

Figure 32. Ignition Delay of Decane and Decane/Al_2O_3 (90/10) Droplets.

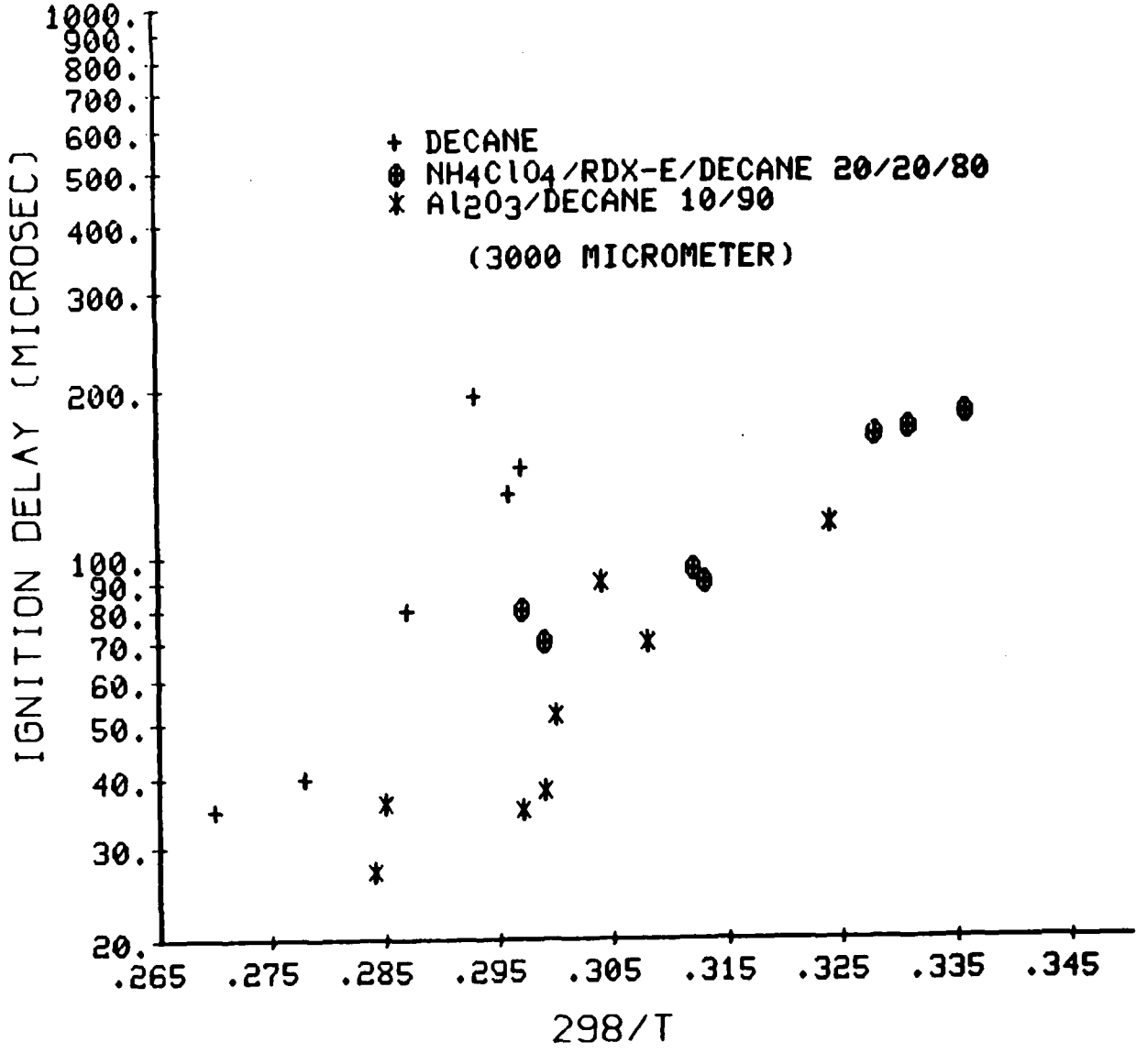

Figure 33. Ignition Delay of Some Droplets.

III. ANALYTICAL STUDIES

A. INTRODUCTION

The main problems associated with dust detonations, which are essentially the same as for gaseous detonations, are:

1) The determinations of the steady-state propagation velocity and the pressure, temperature, and impulse signature generated by a steadily propagating wave.
2) The detonability of various dust air mixtures which, in the case of direct initiation, translates to the minimum energy required to detonate a dust-air mixture.
3) The lean and rich detonation limits which are closely related to the detonability.

However, a number of additional phenomena must be taken into account in dealing with dust detonations. Particularly for high dust loading, two phase flow effects become extremely important within the reaction zone. The combustion of the dust particles is coupled to the convective flow behind the leading shock of the detonation wave. The mechanism of dust combustion is quite different from the burning of premixed gaseous fuel-oxidizer mixtures, and relatively little dust particle reaction rate data is available.

The analytical studies conducted in this program (shared, in part, with another closely related program) have touched on all these problems and have been described in references 2-5. These papers will not be repeated in detail here; however, the relevance of these papers to the problems of dust detonations described above is discussed below.

B. PROPAGATION AND STRUCTURE OF A STEADY-STATE DUST DETONATION

For gaseous detonations with very thin reaction zone lengths, ℓ_R, that is reaction zone lengths which are small compared to the

diameter in detonations propagating in a tube, the detonation velocity, D, is essentially a thermodynamic property of the fuel oxidizer system and can be computed independently of the reaction zone structure. For dust detonations, which generally have long reaction zones because of the slow rate of dust particle burning, this situation is no longer true so that losses from the reaction zone to the tube or other surface bounding the detonation can have a significant effect on the detonation velocity. This problem is treated in reference 2 for the steady-state structure.

After the dust-air mixture passes through the leading shock front of the detonation, the gas decelerates very rapidly while the dust particles, when viewed in shock fixed coordinates continue to move at the detonation velocity. The dust particles decelerate toward the gas velocity in a relaxation region behind the shock. This two phase effect results in an increase in both the gas pressure and temperature. Combustion of the dust particles begins after a certain ignition delay period. The resultant heat release causes an increase in temperature and a reduction in the static pressure. Heat losses to the tube wall and friction can have substantial effects on the propagation velocity D.

The formulation of the equations describing these phenomena is presented in reference 2. Evaluation of the reaction rate parameters in the model used for the combustion of the dust particles is the major source of uncertainty in the calculations. In fact, comparison of the computed reaction zone pressure profiles with measured pressure traces have been used to estimate the rate constants.

An example of computed and measured reaction zone pressure is shown in Fig. 34 for a wheat dust and air mixture. The ignition delay was taken as 10 μsec and the pressure rise in the relaxation zone behind the shock is clearly visible. The reaction zone is an order of magnitude greater than the induction zone. The particle combustion parameters were chosen to provide the best possible agreement between theory and experiment. Agreement is excellent up to about 200 μsec after which the computed

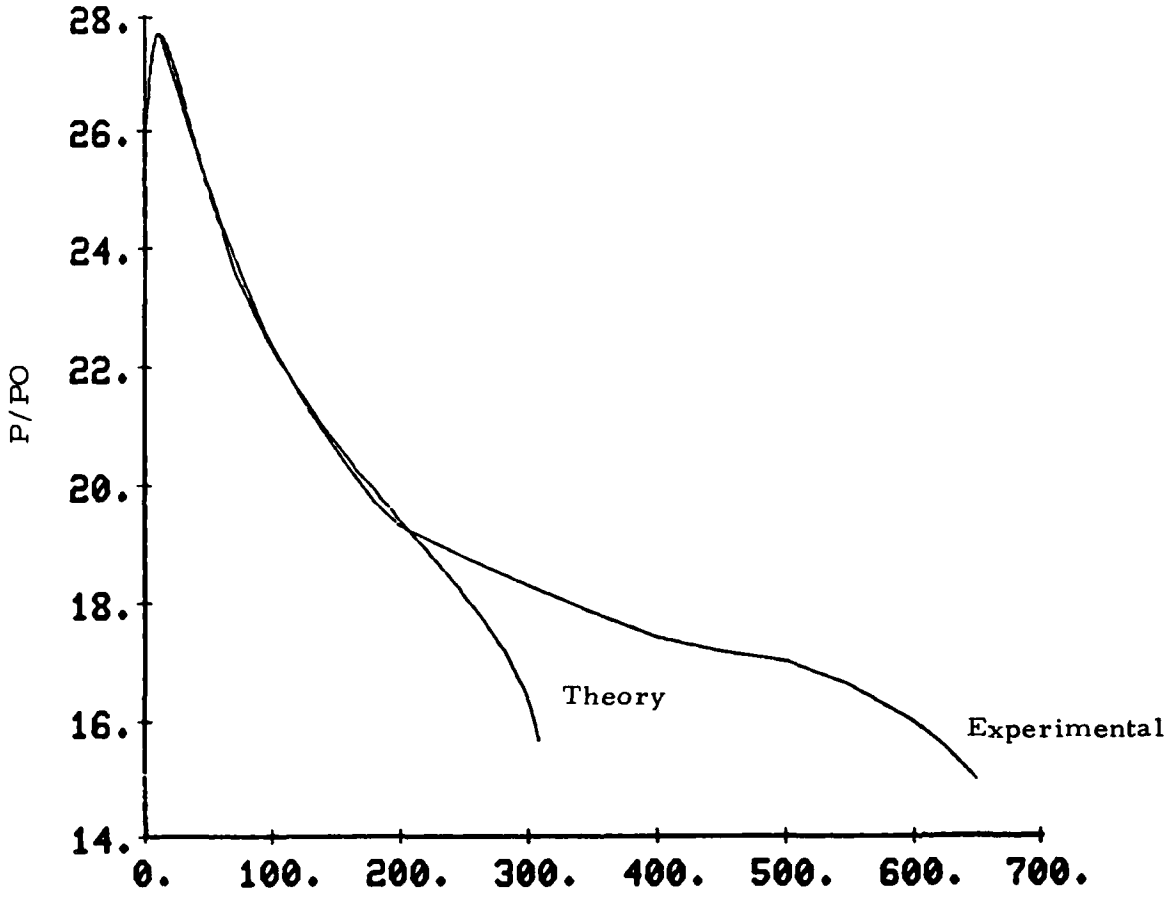

Figure 34. Comparison of computed and experimental pressure profiles.

pressure drops off more rapidly than the measured pressure. Neglect of volatile combustion in the burning model may be responsible for this poor agreement in the late stages of the reaction.

Computed and measured detonation velocities are shown in Fig. 35 as a function of dust concentration and agreement is quite good. The theory makes it possible to compute profiles of other flow properties and to make parametric studies with minimal computing time. As an example, Fig. 36a shows the variation of gas velocity U and particle velocity U_p with time after passage of the leading shock front. It can be seen that the particles decelerate very rapidly and that the gas accelerates due to combustion heat release until the gas velocity exceeds the particle velocity. The variation of temperature and density with distance behind the shock is shown in Fig. 36b.

Detailed calculations of the structure of RDX dust detonations must still be completed. The pressure traces of RDX dust detonations and the results of the calculations in Ref. 5 suggest that the properties of wheat and RDX dusts will be fairly similar. However, the significant result is that a simple model of dust detonations, which can be used for extensive parametric calculations and for the interpretation of experimental data, has been developed.

C. IGNITION DELAY OF DUST PARTICLES BEHIND SHOCK WAVES

The ignition delay distance is a fundamental parameter which has a major influence on the detonability of fuel-oxidizer mistures [6, 7]. The ignition delay of individual dust particles has, therefore, been determined in a shock tube as described in Refs. 3 and 8.

The theoretical calculations of ignition delay are based on the model developed by Ural et al [8]. Particles are assumed to be spherical, and the heart of the analysis is the calcuation of the unsteady temperature distribution within the sphere. Surface heat flux is determined by forced convection due to the relative motion between the particle and the surrounding

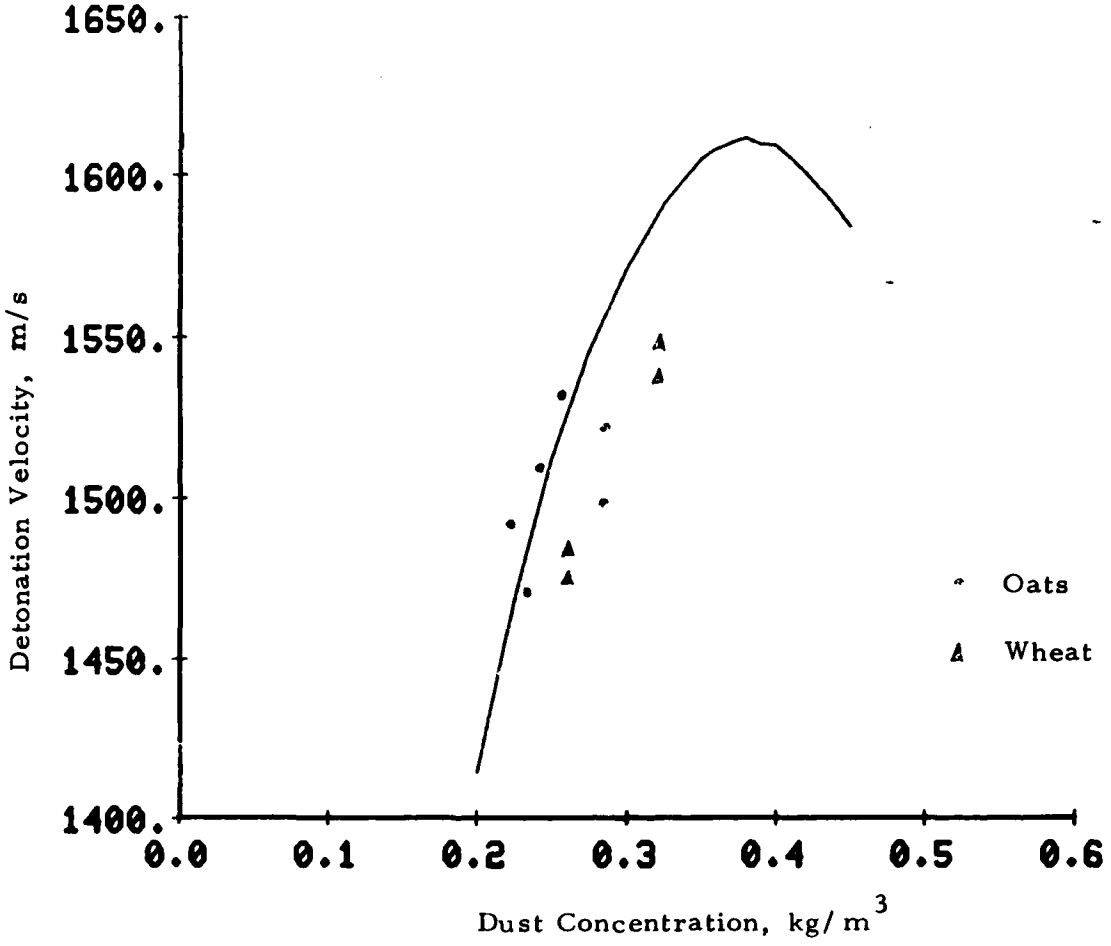

Figure 35. Measured and computed detonation velocities for wheat-air and oats-air mixtures.

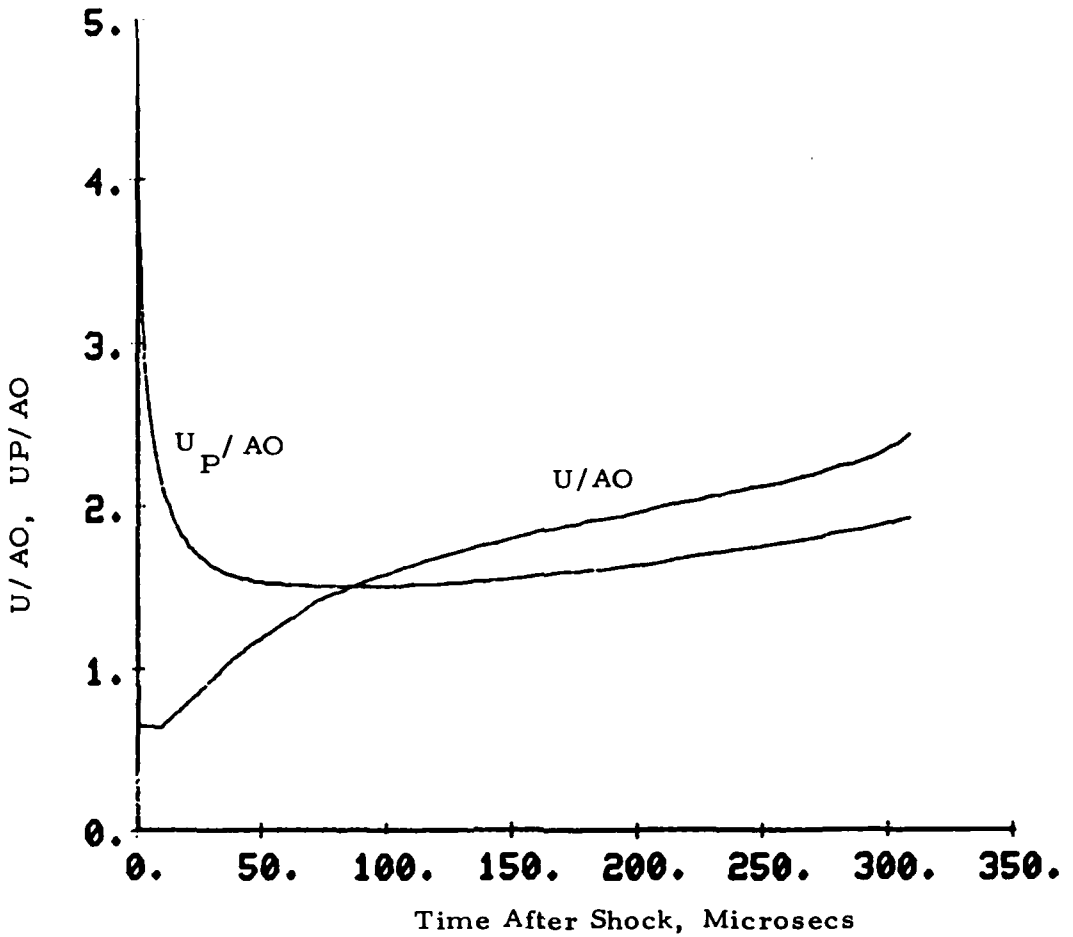

Figure 36a. Particle and gas velocity variation in the reaction zone.

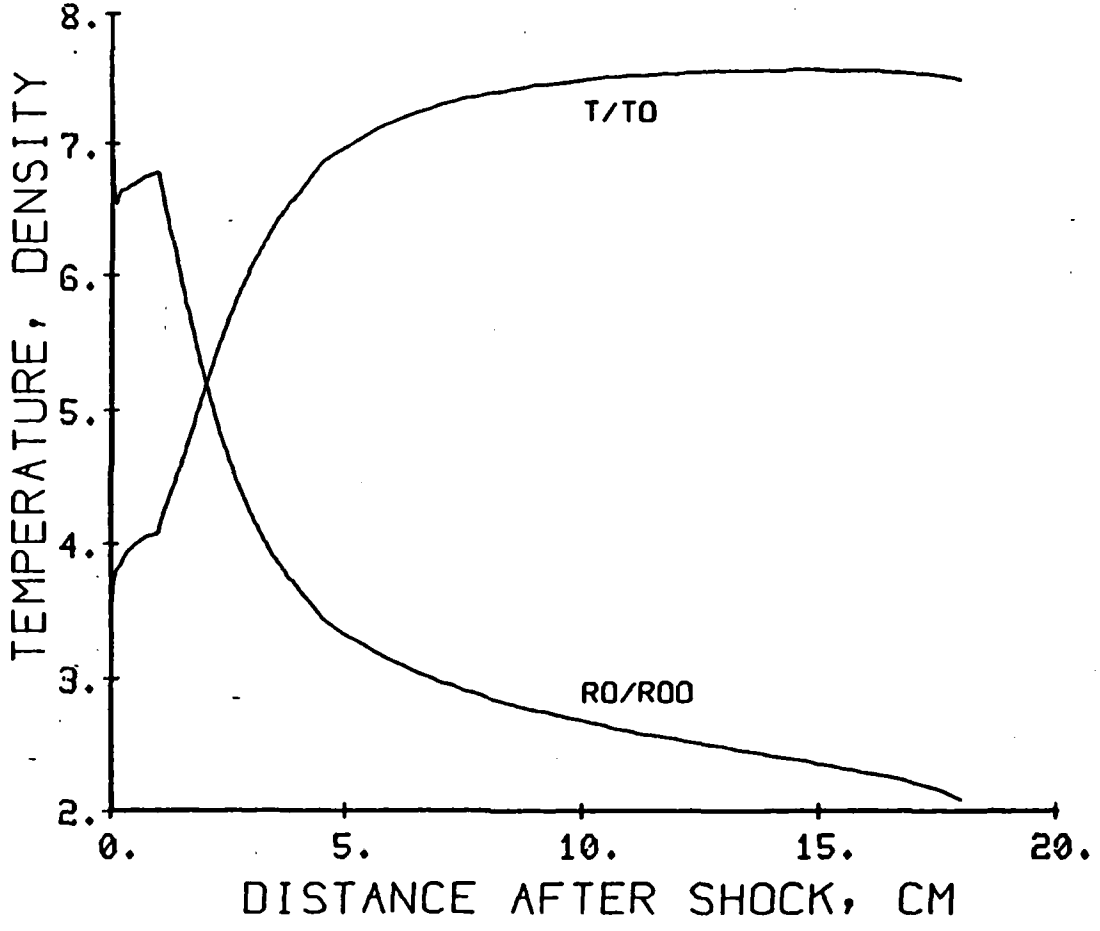

Figure 36b. The variation of reaction zone temperature and density with distance behind the shock.

gas. The forced convection film coefficient depends upon the relative Mach and Reynolds numbers of the particle so that the solution of the heat conduction equation within the particle is coupled to the particle trajectory during acceleration. Volatile burning does not seem to be important during the short delay times characteristic of shock ignition, so that only surface reactions on the particle surface or within the pores for porous materials need to be considered. Ignition is taken to occur at surface temperature runaway, but, as in all such calculations, the combustion model chosen is a major source of uncertainty.

As an example of the results which have been obtained, computed and measured ignition delays for RDX particles are shown in Fig. 37 and agreement appears to be quite good. The computations completed as part of this project indicate that the model of Ural et al [8] provides a reasonable basis for computing particle ignition delays and thus provides a reasonable method for exploring the effect of particle properties and combustion characteristics upon the ignition process. As indicated in Ref. 3, the model can also be used to develop estimates of the acceleration, heating, and reaction times of the particle during ignition and to identify various ignition regimes based on the relative magnitudes of these time scales.

Comparison of the characteristic times for particle surface heating and for chemical reaction suggests that particle ignition occurs as soon as the surface temperature exceeds a certain ignition temperature. Particle ignition thus appears to be tied mainly to the thermal properties and particle heating, and is only slightly dependent on the details of the surface chemistry. This preliminary conclusion is borne out by the ignition delay data which seems to be in a relatively narrow band on the logarithmic plot of ignition delay vs. inverse temperature for a number of different materials.

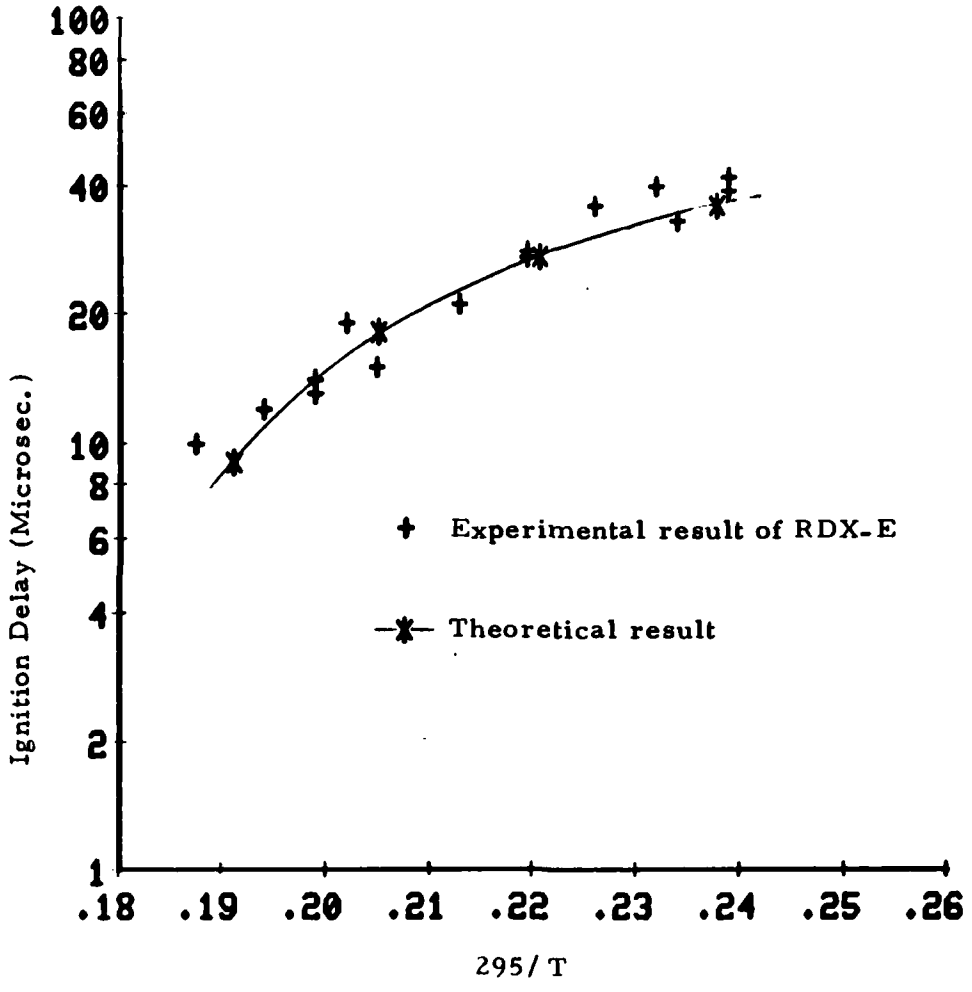

Figure 37. Computed and Measured Ignition Delay Times for 10 μm RDX-E Particles.

D. UNSTEADY PROPAGATION OF DUST DETONATION DURING DIRECT INITIATION

In direct initiation of detonation, a high explosive charge sets up a blast wave which then propagates into the fuel oxidizer mixture. Initiation occurs if the energy released by the high explosive exceeds a certain critical level. During this process, the blast wave will decay to a certain minimum Mach No. and will then re-accelerate to the Chapman-Jouguet Mach number of the fuel-oxidizer mixture. This problem has been discussed by Sichel [6] and by Bach et al [9] in the case of gaseous fuels and by Mitrofanov et al [10] and Cherepanov [11] for spray detonations. Dust detonations have not been considered. The detailed development of the structure of both dust and spray detonations behind a decaying blast wave is explored in Ref. 5 using a numerical code based on the Flux Corrected Transport method, and will have a significant effect upon the initiation process.

The combustion model which has been used assumes that the particle breakup is the rate limiting process, and that gas phase kinetics is instantaneous. The empirical constants of this model are chosen to fit experimental values of the reaction zone length. By using different particle sizes and materials it was possible to explore the wave development for a wide range of reaction zone lengths. For small particles and short reaction zones, on the order of 2 cm, transition to a wave with a structure similar to a gaseous detonation occurred very rapidly; however, for 80 μm RDX particles with a 13 cm reaction zone, the structure was quite different and included a plateau in both the particle and gas velocity, as is evident in Fig. 38 (taken from Ref. 5). Secondary shock waves originating within the reaction zone were observed in the computations for materials with very long reaction zones.

The transition from blast wave to detonation behavior is evident from Fig. 39, also taken from Ref. 5, which shows the variation of pressure behind the leading shock with shock radius for various combustible mixtures. Uncoupling between the combustion front and the leading shock was not

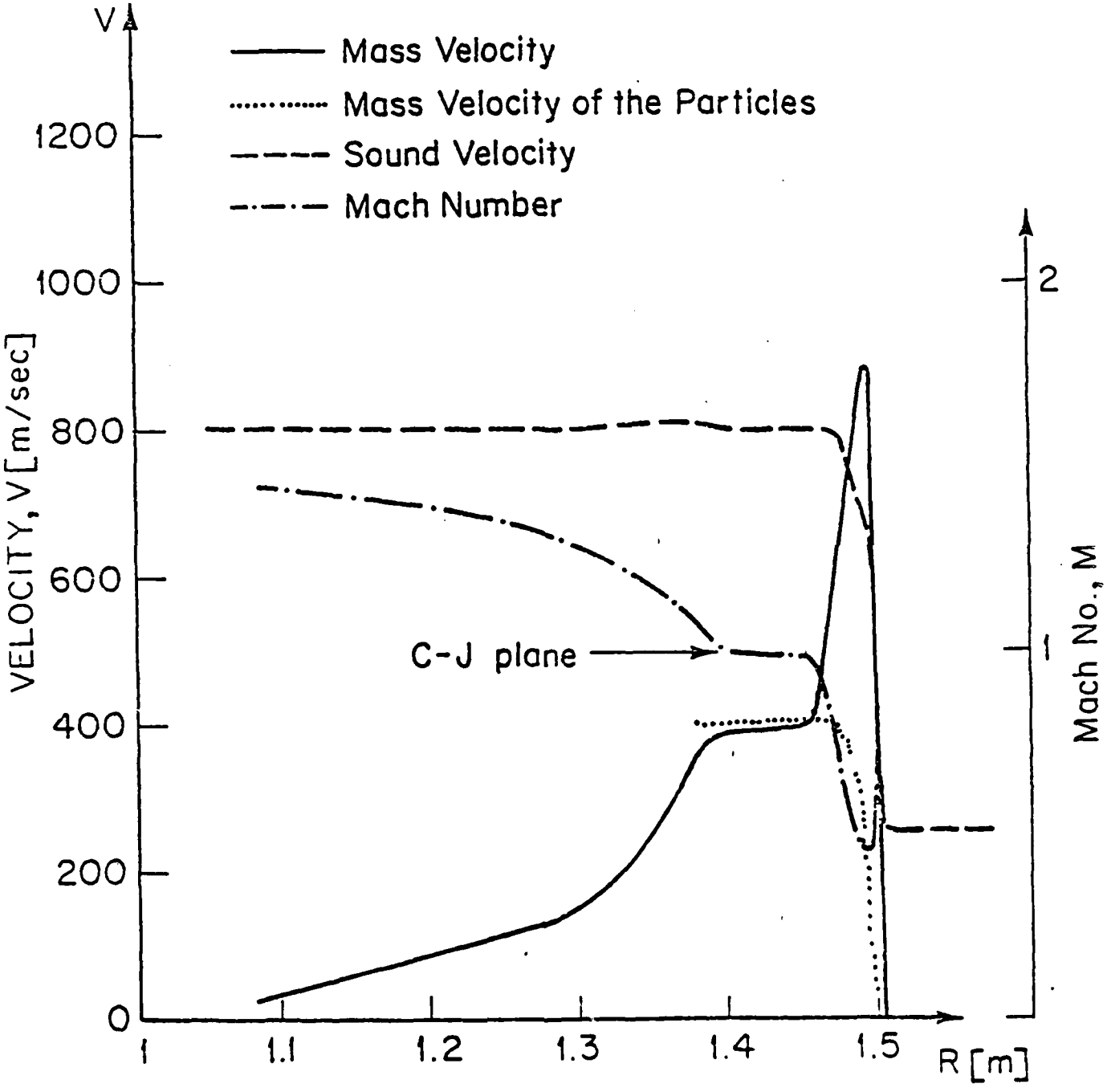

Figure 38. The structure of the detonation wave at a shock radius of 1.5 m for 80 μm RDX particles in air.

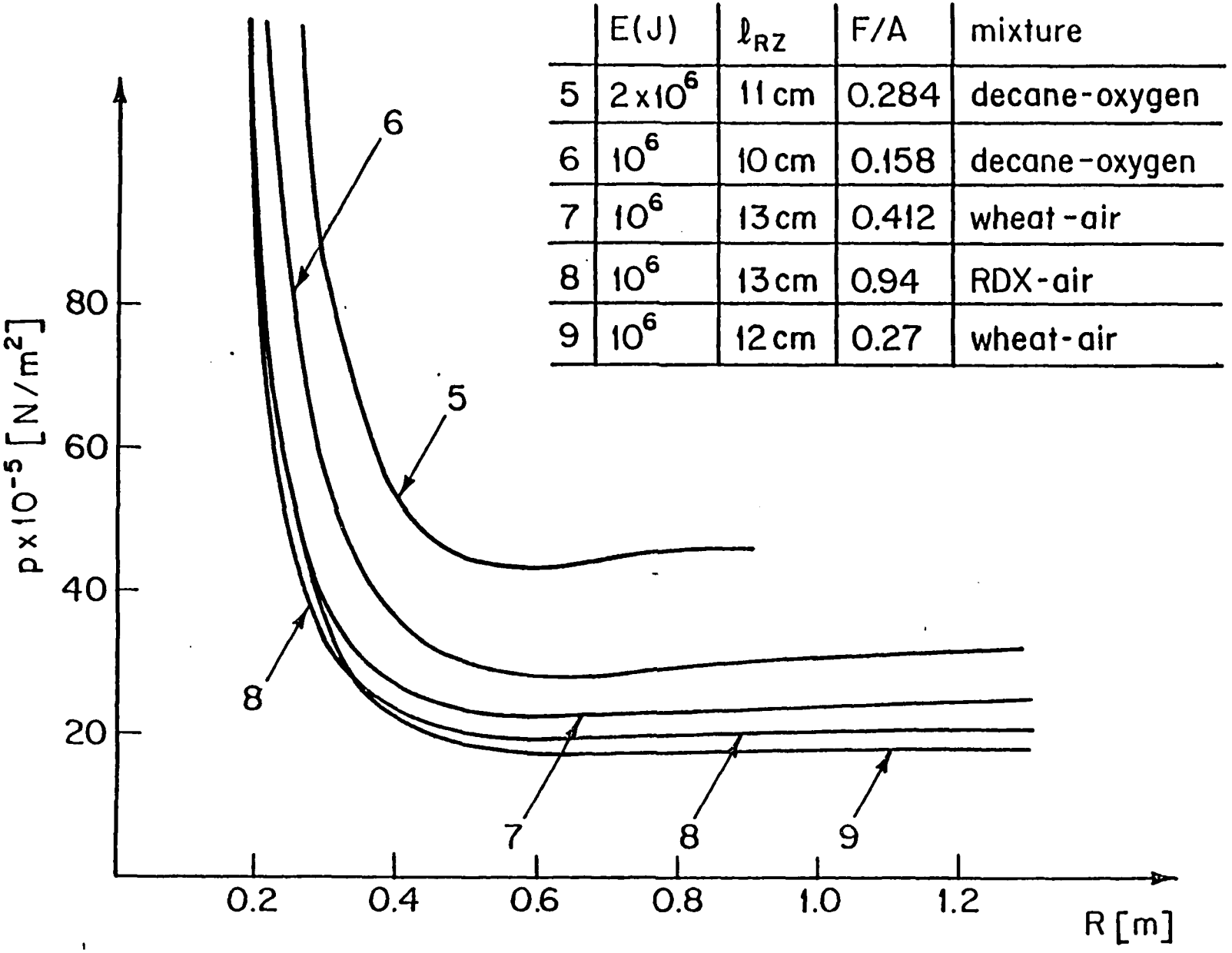

	E(J)	ℓ_{RZ}	F/A	mixture
5	2×10^6	11 cm	0.284	decane-oxygen
6	10^6	10 cm	0.158	decane-oxygen
7	10^6	13 cm	0.412	wheat-air
8	10^6	13 cm	0.94	RDX-air
9	10^6	12 cm	0.27	wheat-air

Figure 39. The pressure behind the leading shock front vs. shock radius for various combustible mixtures.

observed here; evidently because the gas phase Arrhenius kinetics was not taken into account. Comparison of the steady-state reaction zone profiles shown in Fig. 36b and the structure computed from the transient analysis (Fig. 38) shows that the reaction zone thicknesses in each case are on the order of 10 to 15 cm. The variation of particle and gas velocity from the steady-state analysis (Fig. 36a) and from the transient analysis (Fig. 38) are also quite similar when the transient results are converted to shock fixed coordinates. The transient results also show that the gas velocity eventually overshoots the particle velocity.

The dynamic and static impulse generated during the unsteady initiation period also has been determined and is reported in Ref. 4. The impulses generated by RDX-air, decane-oxygen, wheat-air, and point explosions for the same total energy have been compared. Figure 40, taken from Ref. 4, shows the static impulse for RDX, decane, a point explosion and a CJ detonation in a decane-oxygen mixture. It can be seen that RDX produces a larger static impulse than the other mixtures considered. However, since RDX has a low heating value, a much higher fuel-air ratio is required for the same heat release as that generated by the other mixtures. The dynamic impulse was found to closely depend on the detailed structure of the reaction zone of the detonation front. A detailed discussion of the impulse analysis is given in Ref. 4.

E. DISCUSSION OF ANALYTICAL RESULTS

The analytical studies described above have advanced the understanding of the structure and propagation of detonations through RDX dust. Both steady and unsteady propagation has been explored and the factors determining dust particle ignition delay have been investigated. A number of outstanding problems still remain. A precise formulation of the Chapman-Jouguet condition for steadily propagating dust detonations is still needed. The role of the gas phase kinetics of particle combustion in unsteady

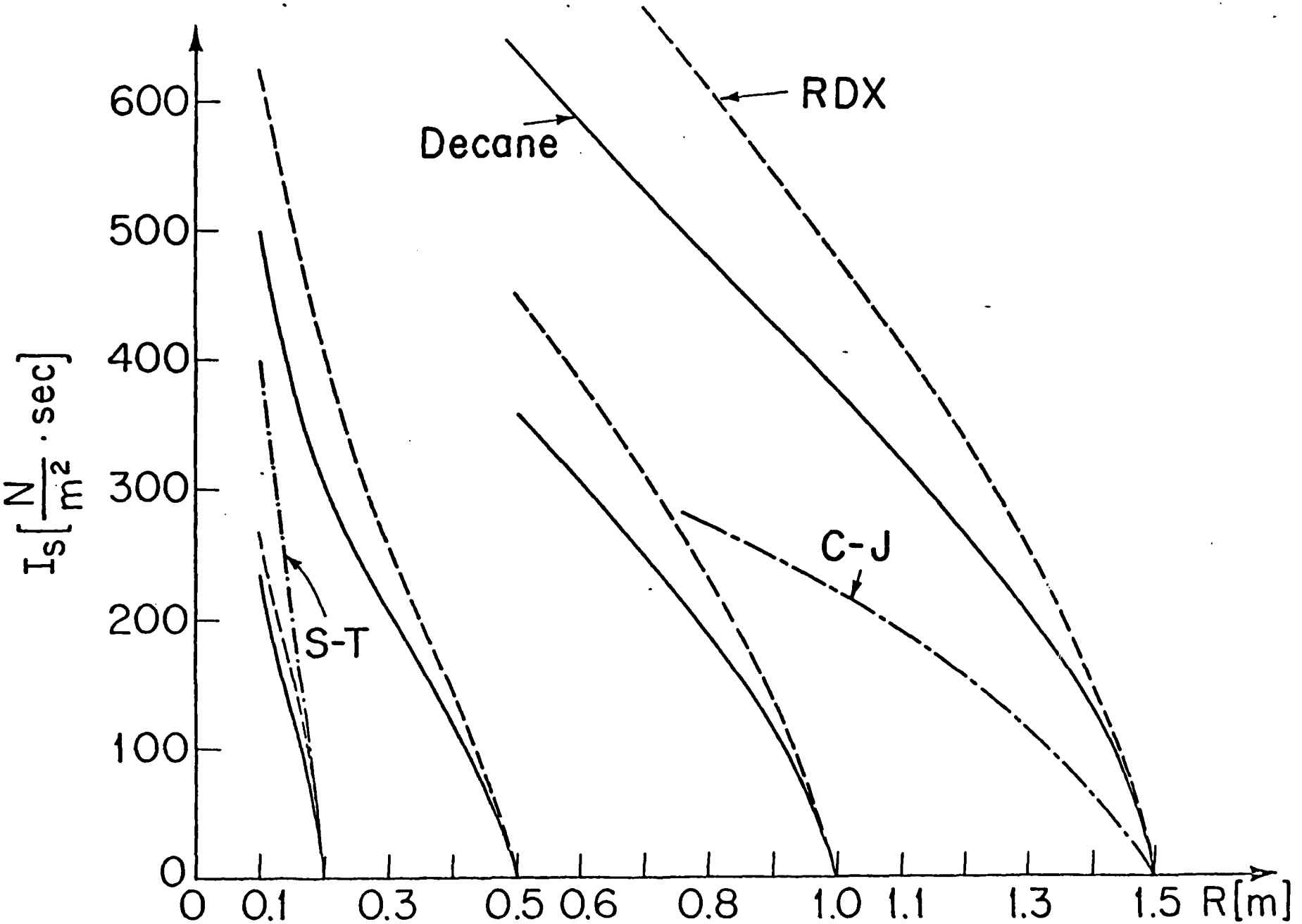

Figure 40. Calculated static impulse vs. radius for decane-oxygen detonation (solid lines), for RDX-air detonation (dashed lines), for point explosion (S-T) and Chapman-Jouguet detonation (C-J).

propagation and extinction must still be determined. Both experimental and theoretical studies of the minimum initiation energies and the detonability limits are still needed. However, the work completed so far will provide the basis for the solution of these additional problems.

IV. SUMMARY

The experimental results presented in the foregoing have shown that RDX dust, when dispersed in air is difficult to detonate, if it can be detonated at all. With some oxygen enrichment (12% O_2, 88% air), large RDX particles (150 μm) were found to detonate but at lower velocities and pressures than theoretically predicted. Small RDX particles (10 μm) could not be detonated even with this enrichment. It is concluded that the inertia of the large particles leads to a large relative velocity between the particles and gas behind the lead shock with the attendant high stagnation temperatures and rapid heating to ignition. Additions of the oxidizing dust, ammonium perchlorate, to the RDX showed an increase in the detonability. The increase in sensitivity was not as great as with increased gaseous oxygen. The thin plastic coating on the RDX particles evidently had some influence on the detonation characteristics. Tests on aged (20 months) small particles showed greater sensitivity.

Many experiments were conducted on the shock wave ignition of liquid fuel drops with suspended dust. It was found that the particles, whether RDX, AP, or inert aluminum oxide, reduced the ignition time over that of the liquid fuel (decane) alone. This would represent an increase in sensitivity.

On the analytical side, a theoretical model was developed for the ignition time delay of dust particles behind a shock wave. This model has shown good agreement with experimental results. An approximate model for the combustion rate of dust, derived in part from the experiments, was used to give a prediction of the propagation rate and structure of a steady-state dust detonation. Numerical calculations were made on the unsteady propagation of a dust detonation when initiated by a blast wave.

REFERENCES

1. Gordon, S. and McBride, B.J., "Computer Program for Calculation of Complex Chemical Equilibrium Compositions, Rocket Performance, Incident and Reflected Shocks, and Chapman-Jouguet Detonation," NASA-SP-273, 1971, Interim Revision, March 1976.

2. Wolański, P., Lee, D., Sichel, M., Kauffman, C.W. and Nicholls, J.A., "The Structure of Dust Detonations" presented at 9th Colloquium on Dynamics of Explosions and Reactive Systems, July 1983, Poitiers, France.

3. Sichel, M., Baek, S., Kauffman, C.W., Maker, B., Nicholls, J.A., and Wolanski, P., "The Shock Wave Ignition of Dusts," abstract accepted for presentation at AIAA 22nd Aerospace Sciences Meeting in January 1984.

4. Eidelman, S., and Sichel, M., "Static and dynamic impulses generated by two-phase detonations," Phys. Fluids, 25, 38 (1982).

5. Eidelman, S., and Sichel, M., "The Transitional Structure of Detonation Waves in Multi-Phase Reactive Media," Comb. Sci. and Tech., 26, 215, (1981).

6. Sichel, M., "*A Simple Analysis of the Blast Initiation of Detonations*," Acta Astronautica, 4, 409, (1979).

7. Lee, J.H., Ann. Rev. Phys. Chem., 28, 75, (1977).

8. E.A. Ural, M. Sichel, C.W. Kauffman, "Shock wave Ignition of Pulverized Coal," Proc. of the 13th International Sympoisum on Shock Tubes and Waves, Niagara Fall, NY, July 6-9 (1981).

9. Bach, G.G., Knystautas, R., Lee, J.H., "Initiation Criteria for Diverging Gaseous Detonations," 13th Symposium (International) on Combustion. The Combustion Institute, Pittsburg, PA, 1097, (1971).

10. Mitrofanov, V.V., Pinaev, A.V., Zhdan, S.A., "Calculations of Detonation Wave in Gas-Droplet Systems," Acta Astronautica, 6, 281, (1979).

11. Cherepanov, G.P., "The Theory of Detonation in Hetrogeneous Systems," Translated from PMTF No. 4, Moscow, April 1965.